Diverse infection models demonstrate robust resistance of *Mycobacterium tuberculosis* to innate immunity

Marian R. Fairgrieve[1], Ella C. Brydon[1], Roberto A. Chavez[1,2], Dmitri I. Kotov[1,5], Russell E Vance[1,2,3,4]*

[1]Department of Molecular and Cell Biology, Division of Immunology and Molecular Medicine, University of California, Berkeley, CA, USA.

[2]Howard Hughes Medical Institute, University of California, Berkeley, CA, USA.

[3]Cancer Research Laboratory, University of California, Berkeley, CA, USA.

[4]Center for Emerging and Neglected Diseases, University of California, Berkeley, CA, USA.

[5]Present address: Division of Infectious Diseases, John T. Milliken Department of Medicine, Washington University, St. Louis, MO, USA.

*Correspondence: rvance@berkeley.edu

Abstract:

Mycobacterium tuberculosis (Mtb) is a robust activator of innate immunity. However, there is little evidence that innate immune mechanisms control Mtb before the onset of adaptive immunity. Prior work has generally used specific pathogen-free (SPF) mouse models and relatively large infectious doses, which may obscure the capacity of innate immunity to control Mtb. Here, we performed ultra-low dose Mtb infections and found that the initial innate immune response was unable to curb even minimal Mtb infectious doses. Additionally, we primed the immune systems of C57BL/6 mice by co-housing with “pet shop” mice prior to Mtb exposure. Co-housed mice were as susceptible to Mtb infection as SPF mice. To more specifically pre-activate innate immunity at the site of Mtb infection, we also infected the lungs of mice with *Legionella pneumophila* (Lp) prior to Mtb. Innate immunity alone can clear large doses (>100,000 CFU) of Lp from the lung within a few days. However, pre-infection with Lp only modestly reduced Mtb CFU compared to mice infected with only Mtb, indicating that Mtb can robustly replicate even in the presence of a strong innate inflammatory response. We performed single-cell RNA-sequencing on myeloid cells from mice either infected with Mtb alone or mice primed with Lp. We found that Lp priming before Mtb infection induced measurable changes in myeloid cells responding to Mtb, but these changes had little effect on innate control of Mtb. Together, these data demonstrate the robust resistance of Mtb to innate immune clearance under diverse experimental conditions.

Author Summary:

Mycobacterium tuberculosis (Mtb) causes more human mortality than any other single pathogen. Despite over 140 years of research, fundamental questions remain about

how Mtb interacts with the immune system during early infection. Interestingly, Mtb is highly immunostimulatory, yet replicates robustly during the innate phase of infection (prior to the onset of adaptive immunity). Using ultra-low dose infections, we show that the innate immune system cannot control infection seeded by even a single bacterium, and that innate immune pathways which aid in control during later disease stages fail to exert control during the early innate phase. To test whether the lack of innate control of Mtb is due to insufficient inflammation during the critical early days of infection, we primed the innate immune system using pet shop co-housing and *Legionella pneumophila* co-infections. However, priming failed to inhibit early Mtb growth. Our results suggest that although Mtb is capable of inducing robust inflammatory responses, it exhibits potent intrinsic resistance to anti-bacterial innate immune responses.

52 **Introduction**

53 Mtb robustly engages and activates innate immune cells. Diverse pattern-recognition
54 receptors (PRRs) including Toll-like receptors, inflammasomes, NOD1/2, cGAS and
55 dectin receptors all detect and respond to Mtb infection[1]. Engagement of PRRs by Mtb
56 results in a robust inflammatory response. *In vivo*, Mtb initially infects and replicates
57 within alveolar macrophages (AMs), which are thought to provide a permissive niche for
58 Mtb replication in the initial days post-infection, while simultaneously inducing pro-
59 inflammatory responses[2-4]. Contained Mtb (co-Mtb) or BCG vaccination infection
60 models can further enhance pro-inflammatory responses[5-7]. However, in naïve, co-
61 Mtb, or BCG-vaccinated mice, Mtb will replicate many thousand-fold prior to the onset of
62 adaptive immune control, which occurs starting after day 14. Genetic evidence also
63 supports the conclusion that Mtb is largely resistant to early innate immune responses.
64 Mice with genetic deficiencies in the innate immune response have nearly identical CFU
65 burdens to wild type mice before the onset of adaptive immunity[8-17]. The existing data
66 therefore suggest that although Mtb elicits a robust innate inflammatory response, Mtb
67 replication is unrestricted during the early innate immune response.

68 The failure of innate immunity to control Mtb infection in the lung is not due to an
69 intrinsic inability of the lung to control bacterial infections. Indeed, even large doses
70 (>10^5 CFU) of other pathogenic bacteria, including *Pseudomonas aeruginosa* and
71 *Staphylococcus aureus* are readily and rapidly cleared from the lungs of mice[18, 19].
72 *Legionella pneumophila* (Lp) provides a particularly interesting example of a bacterial
73 pathogen that is readily cleared by innate immune responses in the lung. Like Mtb, Lp
74 initially infects alveolar macrophages and engages a very similar set of host pattern
75 recognition receptors (the LPS of Lp does not activate TLR4) [20-22]. However, in

contrast to Mtb, which establishes chronic infections even after an initial inoculum of 1-3 CFU, doses as high as 10^6 CFU of Lp are cleared from the lungs of SPF C57BL/6 mice within 3-5 days post-infection[23, 24]. Interestingly, many of the key innate pathways known to be critical for Lp clearance, such as TNFα, IL-1, and IFNγ, are also elicited by Mtb and help control infection, but during the adaptive phase of the response (post-day 14) instead of during the innate phase[25-27].

Most studies of Mtb infection in mice have been performed with specific pathogen-free (SPF) C57BL/6 mice, using doses 20-100 times the infectious dose 50 (ID50), which is as low as 1 CFU in mice[24, 28]. Ultra-low dose (ULD) Mtb infections have been used as a promising model for evaluating BCG vaccine efficacy in mice, suggesting that the ULD infection model could be used as a sensitive method to uncover *in vivo* mechanisms of Mtb control[29]. In addition, laboratory mice kept in clean SPF facilities have underdeveloped immune systems compared to wild, or pet shop raised mice[30]. When C57BL/6 mice are co-housed with pet shop mice, their immune systems mature to more closely resemble the activation state of the immune system of adult humans, with increased numbers of circulating monocytes, macrophages, neutrophils, and memory T cells[30, 31]. Co-housing SPF mice with pet shop mice can strongly enhance protection against certain intracellular bacterial infections, though this effect is variable[32].

In this study, we systematically investigated whether the use of more physiologically relevant animal models could reveal a role for innate immunity in control of Mtb. First, we used an ULD infection model to test whether high infectious doses used in previous studies had obscured a potential contribution of innate immunity to Mtb control[24]. However, we found no evidence that innate immunity controls Mtb even at

100 ultra-low infectious doses. Additionally, as an alternative approach to enhance innate
101 responses, we primed the innate immune system through either pet shop mouse co-
102 housing or Lp co-infection. Although scRNA-seq revealed that Lp-priming substantially
103 altered the innate response to Mtb, we found no evidence that a primed innate immune
104 system impaired Mtb replication during the innate phase of the infection. Together, our
105 results indicate that Mtb robustly resists innate immune clearance mechanisms in the
106 lung, even under experimental conditions where the innate response should be favored,
107 such as during ultra-low dose infections or conditions in which lung immune responses
108 are already primed.
109

110 **Results**

111 Even at ultra-low doses, innate immunity does not control Mtb

112 We hypothesized that non-physiological infectious doses of Mtb used in
113 conventional mouse infections may have overwhelmed the mouse innate immune
114 system, thereby obscuring the contribution of innate immunity to Mtb control. To
115 sensitively test of the ability of innate immunity to control Mtb, we used a previously
116 described method to infect wild-type C57BL/6J mice with ultra-low doses (1-3 CFU) of
117 Mtb (Erdman strain)[29]. To assess whether innate immune responses restrict Mtb at
118 these ultra-low doses, in parallel we also infected *Ifngr1*$^{-/-}$, *Tnfr*$^{-/-}$, *Sp140*$^{-/-}$, *MyD88*$^{-/-}$
119 *Trif*$^{-/-}$, and *Atg5*$^{fl/fl}$ *LysM-Cre*$^{+}$ mice. These mice lack key factors involved in innate
120 immunity, but prior work with conventional doses had only previously documented their
121 importance in Mtb infection during the adaptive phase[33-37]. We reasoned that use of
122 ultra-low doses may reveal a phenotype for these knockout mice during the innate
123 phase (i.e., by day 14). In all cases, however, the immune-deficient mice had

124 comparable CFU to control wild-type mice at 14 days post-ultra-low dose infection
125 (Figure 1A-E). In addition, the fraction of mice that were successfully infected (i.e.,
126 harboring detectable CFU on day 14) were not significantly different when comparing
127 wild type to immune-deficient animals (Table 1). In these experiments, 32%-68% of the
128 mice remained uninfected across experiments (Table 1), consistent with an ultra-low or
129 near ultra-low infectious dose (1-3 CFU)[24, 38]. Thus, the innate immune response to
130 Mtb appeared to be remarkably ineffective *in vivo* and failed to control infections seeded
131 by 1-3 bacteria.
132
133 Priming C57BL/6 mice with pet shop mouse co-housing does not alter control of Mtb
134 We sought to test the hypothesis that innate immunity does not contribute
135 significantly to initial Mtb control (up to day 14 post-infection) in SPF mice because the
136 innate immune compartment is insufficiently matured or primed prior to Mtb infection. To
137 mature the immune system of SPF mice, we employed a previously described pet shop
138 mouse co-housing model[30]. We purchased female mice from a local pet shop in
139 Berkeley, CA and co-housed them with female SPF B6 mice for 60 days. Serological
140 surveys for common mouse pathogens were performed, and pet shop mice indicated
141 the presence of numerous pathogens including helicobacter, mouse parvovirus, murine
142 norovirus, and rotavirus. The presence of pathogens was heterogenous across
143 individual mice (Supplemental Table 1). Co-housed mice displayed symptoms of
144 pathogen exposure, including weight loss, particularly in the first 10 days of co-housing
145 (Supplemental Figure 1).
146 We measured the impact of co-housing by examining the number of innate and
147 adaptive cells in the lung by flow cytometry after 60 days of co-housing (Figure 2A). Co-

148 housing did not have profound effects on the innate immune cellular compartment in the
149 lung at day 60 (Figure 2B). However, at this timepoint, there were significant differences
150 in the number of $CD4^+$ and $CD8^+$ effector memory cells (Figure 2C), similar to the
151 changes observed in a previously published study of pet shop mice[30, 32]. These
152 changes varied by cage, with formerly SPF mice more closely resembling the pet shop
153 mouse with which they were co-housed than they resembled other pet shop or SPF
154 mice (Supplemental Figure 2A-D).

155 To confirm that our pet shop mouse co-housing procedure could enhance innate
156 immune control of bacterial infections[31, 32], we infected age-matched SPF and co-
157 housed mice with *Listeria monocytogenes* (Lm). In both the liver (Figure 3A) and spleen
158 (Figure 3B), co-housed mice exhibited significantly lower CFU at 48 hours post-infection
159 compared to SPF mice. We also infected mice intranasally with Lp. Interestingly, co-
160 housed mice generally did not have significantly lower Lp CFUs at 48 hours post-
161 infection, but this varied by cage (Figure 3C, Supplemental Figure 2E).

162 We then infected a cohort of pet shop co-housed mice and matched SPF
163 controls with Mtb. Because the number of surviving mice co-housed with each pet shop
164 mouse was limited, we employed a standard low dose of 20-50 CFU to ensure all mice
165 in each group were infected, and measured lung CFU at 7-, 14-, and 21-days post-
166 infection. We found that co-housed and SPF mice contained similar numbers of CFU in
167 the lungs (Figure 3D). Strikingly, the Mtb infections were very consistent, and CFUs did
168 not vary substantially by cage, unlike mice infected with Lm or Lp.

169 We assessed the numbers of innate and adaptive immune cells in the lungs at 14
170 days post-Mtb infection (Figure 3E-F). The results of the co-housed mice were highly
171 variable compared to SPF mice, reflecting the variation seen in uninfected co-housed

172 mice (Figure 2B-C). The numbers of innate (Figure 3E) and adaptive (Figure 3F) cells
173 also varied between co-housing experiments. Overall, the flow cytometry data suggests
174 that co-housing induced small changes to the composition of immune cells in the lung
175 by day 14 post-infection. Together, our findings imply that co-housing with pet shop
176 mice induces an altered immune state in SPF mice that can variably promote innate
177 immune control of infections, but that Mtb is resistant to this shift.
178
179 Mtb exhibits robust replication despite priming the innate immune system with *L.*
180 *pneumophila*
181 Pet shop mice carry an array of viruses, bacteria, and parasites. The priming
182 effects of these diverse pathogens may vary substantially or even counteract each
183 other. Some may promote anti-bacterial immunity in the lung, whereas others may
184 hinder it. In addition, each pet shop mouse may carry or transmit a distinct combination
185 of pathogens, and it is therefore difficult to conduct controlled experiments. Moreover,
186 although pet shop co-housing reduced systemic Lm colonization and increased the
187 number of activated lymphocytes in the lung, there were inconsistent effects on Lp
188 clearance in the lung. Therefore, it was unclear whether pet shop co-housing
189 consistently induced an anti-bacterial innate immune response in the lung.
190 We therefore turned to co-infections with Lp, a pathogen that is established to
191 elicit a robust and highly effective anti-bacterial innate immune response in the lung
192 (Supplemental Figure 3A-C). Co-infections with Lp avoided the complexities of co-
193 housing and allowed us to activate innate immune responses without eliciting
194 confounding antigen-specific anti-Mtb adaptive immune responses. Lp also infects and
195 is cleared from the same cell type (alveolar and interstitial macrophages) that Mtb

196 infects during the initial innate phase of infection (Supplemental Figure3C). We infected
197 mice with JR32, a clinically-derived isolate of Lp[39]. Lp secretes flagellin into the
198 cytosol of infected host cells, resulting in activation of the NAIP–NLRC4 inflammasome
199 and induction of rapid pyroptotic cell death[40, 41]. To avoid killing alveolar
200 macrophages, we infected mice with Lp lacking *flaA* (Lp∆*flaA*, hereafter referred to as
201 Lp), which does not activate NAIP–NLRC4-mediated pyroptotic cell death[40, 41]. To
202 confirm that priming with flagellin-deficient Lp enhances clearance of subsequent
203 bacterial infections, we infected mice with Lp, followed by a second Lp infection 2 days
204 later (Figure 4A). Each infection was performed with a strain bearing a unique antibiotic
205 resistance marker so the strains could be distinguished. While previous infection with Lp
206 does not reduce the initial CFU that reach the lung during a secondary infection, we
207 found that priming with Lp results in approximately 3-log lower CFU in the lungs 2 days
208 post-secondary Lp infection compared with unprimed mice (Figure 4B). This implies that
209 priming with Lp strongly activates an anti-bacterial innate immune response.
210 We then tested whether priming the lung with Lp could enhance control of Mtb
211 compared to unprimed mice (Figure 4C). We first infected mice intranasally with 10^5
212 CFU of Lp. At 3 days post-Lp infection, when Lp had largely been cleared by the innate
213 immune system (Supplemental Figure 3A), we then infected mice with approximately 10
214 CFU of Mtb via the aerosol route. At both 1 and 14 days post-Mtb infection, we
215 compared Mtb CFU between unprimed mice, which were infected only with Mtb, and
216 Lp-primed mice. Lp priming did not affect the initial number of Mtb bacilli that reach the
217 lung. Strikingly, priming did not influence Mtb burdens in the lung at 14 days post-
218 infection (Figure 4D). Notably, Lp priming did reduce Mtb dissemination to the spleen at
219 14 days post-infection, suggesting it induced an immune response that partially

220 restricted extra-pulmonary dissemination or replication (Figure 4E). These results
221 indicate that Mtb was able to replicate even in the potently anti-bacterial lung
222 environment induced by Lp priming. To determine whether Lp priming persistently
223 affected the lung immune compartment after Mtb infection, we measured innate immune
224 cells in the lungs by flow cytometry (Figure 4F). Similarly to the results in co-housed
225 mice (Figure 3E-F), after 14 days of Mtb infection, there were similar numbers of
226 neutrophils, interstitial macrophages (IMs), monocytes, and alveolar macrophages
227 (AMs), in Lp-primed mice compared to unprimed mice. Together, our data suggest that
228 Mtb is able to replicate even in mice where anti-bacterial innate immune responses are
229 strongly activated.
230
231 Prior Mtb infection does not impact clearance of Lp
232 Mtb may impair effective innate immunity by suppressing innate immune
233 responses[3, 4]. We sought to address this possibility by infecting mice with a ~400
234 CFU dose of Mtb, allowing the infection to progress for 14 days, and then infecting
235 these mice (or control uninfected mice) with Lp (Figure 4G). At 2 days post-Lp infection,
236 there was no difference in Lp lung CFU comparing Mtb-infected and Mtb-uninfected
237 hosts (Figure 4H). This experiment does not address local or cell-intrinsic
238 immunosuppressive effects as Lp and Mtb are unlikely to infect the same cells but does
239 suggest that Mtb does not induce a globally immunosuppressive environment in the
240 lung.
241
242 Single cell RNA-sequencing reveals changes to myeloid cell compartment after Lp-
243 priming

244 To further characterize the effect of bacterial priming on innate immune
245 responses to Mtb, we performed scRNA-seq on myeloid cells isolated from the lungs of
246 unprimed and Lp-primed mice infected for 14 days with Mtb at an initial dose of ~50
247 CFU (Figure 5A). CD64-positive cells were magnetically enriched, sort purified, and
248 processed for library generation with the 10X Genomics platform. Mtb-infected and
249 uninfected bystander cells were sorted. However, at this low initial dose and early time
250 point, there were insufficient numbers of Mtb-infected cells to perform scRNA-seq.
251 Therefore, we solely analyzed bystander cells. Protein expression was measured
252 concurrently with mRNA by employing CITE-seq, allowing for weighted nearest
253 neighbor (WNN) analysis to cluster cells on mRNA and protein expression and WNN
254 uniform manifold approximation and projection (wnn.UMAP) reductions for data
255 visualization (Supplemental Figure 4A, B)[42]. Confirming the efficiency of our
256 enrichment procedure, most cells isolated were myeloid cells, with only ~10% of cells
257 expressing other cell markers. The five AM clusters (Supplemental Figure 4A) were re-
258 clustered into one cluster for downstream analysis (Figure 5B).
259 All clusters were represented in both datasets. Unprimed mice exhibited
260 significantly elevated Interferon-stimulate gene (ISG)-expressing macrophages and Lp-
261 primed mouse lungs contained significantly higher numbers of $CD86^{+}$ interstitial
262 macrophages (FDR < 0.05 and mean Log2 Fold Enrichment > 0.58) (Figure 5C)[43].
263 When we examined the differential gene expression of all the cells in the dataset, we
264 found that unprimed mice significantly upregulated genes associated with type I and
265 type II interferon (IFN) signaling, including *Isg15*, *Cxcl10*, and IFIT family members
266 (Figure 5D, Supplemental Figure 4C). By contrast, Lp-primed mice induced genes

267 associated with inflammation, but also control of inflammation such as *Apoe* and *Trem2*
268 (Figure 5D, E)[44].
269 Overall, our data reveals that Lp infection results in persistent effects on the
270 myeloid cell compartment that are evident even after 14 days of Mtb infection, well after
271 Lp itself has been cleared. However, these differences in innate immune signaling do
272 not dramatically alter the growth of Mtb bacteria, suggesting that Mtb replication is
273 largely unaffected by a variety of anti-bacterial innate immune responses.
274

275 **Discussion**

276 In mice, the initial *in vivo* innate immune response to Mtb fails to prevent the
277 expansion of Mtb from a few bacilli to more than 10^5 bacilli within 14 days (Figure 1)[24].
278 This rate of expansion corresponds to an approximate doubling time of 24h, similar to
279 the doubling rate in rich media. In nonhuman primate infections, individual Mtb bacilli
280 can also replicate largely unrestrained for several weeks[28, 45]. However, after the
281 onset of adaptive immunity, innate immune clearance mechanisms—such as the
282 microbicidal activity of macrophages—are critical restriction of Mtb, as mice with genetic
283 deficiencies in innate immunity eventually exhibit rapid decline as well as loss of
284 bacterial control[9, 10, 36, 46]. Mtb control during the adaptive phase has largely been
285 attributed to enhanced macrophage activation following the increase of IFN-γ production
286 by $CD4^+$ T cells, though control of Mtb after the onset of adaptive immune activation is
287 only partially dependent on IFN-γ, implying other pathways are also at play[47-50].
288 Patients with Mendelian Susceptibility to Mycobacterial Disease (MSMD) typically carry
289 genetic mutations in IFN-γ-related pathways[51-53], further emphasizing the role of
290 innate immunity in mediating successful adaptive immune responses to Mtb.

291 Human Mtb infections are also presumably poorly controlled by the innate
292 immune system alone, though this is difficult to demonstrate experimentally. So-called
293 “resisters”, who remain persistently negative by interferon-gamma release assay (IGRA)
294 and tuberculin skin test (TST) despite exposure to Mtb, had been thought possibly to
295 clear Mtb with innate immunity alone[54]. However, recent publications have
296 demonstrated that these individuals likely control Mtb infections with alternative adaptive
297 immune responses that were not detected by these diagnostic tests[55-57]. Studying
298 the characteristics of the human innate immune response to Mtb poses challenges due
299 to the difficulty in identifying recently infected individuals and assessing the localized
300 responses within their lungs.

301 In this study, we sought to employ alternative Mtb infection models to see
302 whether they might reveal innate immune mechanisms of Mtb control. We first
303 employed a previously described ULD infection model[24]. ULD infections clearly
304 demonstrated that the innate immune system alone is unable to clear or even control
305 infections seeded by even 1-3 bacilli, indicating that the size of the initial infectious dose
306 is not the limiting factor for innate immune control of Mtb *in vivo*. Wild-type mice and
307 mice harboring mutations in key genes critical for Mtb control (e.g., *Ifngr1*, *Myd88*, *Atg5*,
308 *Tnfr1*, and *Sp140*) had comparable CFU in the lungs at 14 days post ULD-infection, and
309 the fraction of infected mice were not significantly different when comparing wild-type to
310 immune-deficient animals. These results suggest that genes known to play important
311 roles in Mtb control do not exert substantial effects during the innate phase of the
312 infection, even at highly limited infectious doses.

313 We attempted to enhance innate immune responses to Mtb by pet shop mouse
314 co-housing and by Lp co-infections. Pet-shop co-housed animals have previously been

315 shown to exhibit enhanced control of *Listeria[31]*. In addition, we reasoned that since
316 high doses of Lp are rapidly cleared from the lung within a few days, Lp must elicit a
317 highly effective anti-bacterial innate immune response, and we wondered whether this
318 response would have any effect on the control of Mtb. Use of Lp also negated the
319 possibility of inducing Mtb-specific adaptive immune responses that might confound the
320 results. However, these approaches also failed to substantially enhance innate immune
321 control of Mtb replication. We conclude that innate immunity exhibits a limited capacity
322 to control Mtb, even if primed before Mtb exposure.

323 Importantly, Mtb alone can also induce inflammatory innate immune responses.
324 Therefore, it was possible that Lp priming did not greatly affect Mtb clearance because
325 Lp priming did not enhance or change innate immune responses over and above those
326 elicited by Mtb alone. Indeed, by both flow cytometry and scRNA-seq, we demonstrated
327 the cellular innate immune response to Mtb in naïve and Lp-primed mice was generally
328 similar, characterized by the presence of neutrophils, monocytes, and macrophages to
329 the lung. However, our scRNA-seq experiment revealed some notable differences in
330 cell populations and interferon responses between Lp-primed and unprimed mice. Lp-
331 primed mice exhibited an increase in macrophages expressing CD86, a cell-surface
332 protein that provides co-stimulation to T cells[58, 59]. Interestingly, CD86 is reduced in
333 TB patients compared to healthy controls[60], though given its role in T cell co-
334 stimulation, it is likely that CD86 acts primarily via adaptive rather than innate immunity.
335 In addition to CD86+ macrophages, Lp-primed mice expressed genes associated with
336 later stages of inflammation and with regulation of inflammation (Figure 5D, E).
337 Because of the 3-day pre-exposure to Lp prior to 14 days of Mtb infection, Lp primed
338 mice have been infected for a total of 17 days, versus only 14 days for the Mtb-only

339 infected mice. The differences we see in Lp-primed mice may therefore reflect a more
340 advanced progression of the immune response in these mice versus unprimed mice.
341 scRNA-seq also revealed that unprimed, Mtb-infected mice possessed a
342 population of ISG-expressing macrophages and showed upregulated ISG expression
343 compared to Lp-primed mice. In both mice and humans, type I IFN can be associated
344 with immunosuppression and progression of TB [61]. In humans, type I IFN precedes
345 active infection, and deficiencies in the type I IFN receptor are associated with
346 protection from TB [62, 63]. C57BL/6 mice do not robustly recapitulate the IFN-driven
347 TB susceptibility, due to the activity of the nuclear body protein Sp140 [35, 64].
348 However, despite the reduced expression of type I IFN, even in wild-type C57BL/6 mice
349 type I IFN signaling impairs responsiveness to IFN-γ and IL-1, both of which are critical
350 to the control of Mtb [63, 65, 66]. However, *Ifnar*$^{-/-}$ mice show only mild resistance to
351 Mtb, and no difference of control in the lung during the innate immune phase [67]. The
352 role of type I IFN in wild-type mice is not well established, but we hypothesize that
353 during the innate phase of the immune response, induction of type I IFN signaling may
354 aid Mtb in establishing an infection in the lung. The mechanism of dampened ISG
355 induction following Lp priming compared to unprimed, Mtb-infected mice, despite the
356 known ability of Lp to induce ISG expression, remains unclear, but may reflect an
357 immunoregulatory feedback loop [68, 69].
358 Flow cytometry and scRNA-seq analyses revealed that Mtb infection triggered a
359 potent innate immune response. Our data demonstrate the robust resistance of Mtb to
360 innate immunity under diverse experimental conditions. Although Mtb may evade or
361 impair the induction of specific innate immune pathways, the innate response to Mtb is
362 overall robust and is characterized by the recruitment of cells and induction of an

363 inflammatory response that is highly effective against other lung pathogens, such Lp.
364 We therefore propose that a major reason for the failure of innate immunity to control
365 Mtb is the robust resistance of Mtb to cellular stress and damage. Mtb exhibits
366 resilience against antimicrobial effector such as reactive oxygen, nitrogen species, and
367 aldehydes, likely through intrinsic mechanisms such as its thick and waxy
368 mycomembrane, a slow replication rate, and effective repair systems [70-72]. These
369 characteristics have earned Mtb the epithet “the honey badger of pathogens”[73]. Like
370 the honey badger that famously resists cobra venom or porcupine quills, Mtb appears
371 impervious to the anti-bacterial arsenal that can rapidly clear other infectious agents[74].
372 This exceptional resistance to innate immune effectors may be an important factor
373 contributing to the extraordinary success of Mtb as a human pathogen.
374

375 **Materials and Methods**

376 Animals

377 Mice were maintained under specific pathogen free conditions and housed at 23°C with
378 a 12-hour light-dark cycle in accordance with the regulatory standards of the University
379 of California Berkeley Institutional Animal Care and Use Committee. All mice were 6-12
380 weeks old at the start of procedures. C57BL/6, B6.129S7-Ifngr1tm1Agt/J *(Ifngr1$^{-/-}$),* and
381 B6.129S-*Tnfrsf1b^{tm1Imx} Tnfrsf1a^{tm1Imx}*/J *(Tnfr$^{-/-}$)* mice were purchased from Jackson
382 Laboratories. *Atg5$^{fl/fl}$-LysM^{Cre}* and *Atg5$^{fl/fl}$* and mice were provided by Jeffery Cox at the
383 University of California, Berkeley. *MyD88$^{-/-}$Trif$^{-/-}$* mice were provided by Gregory Barton
384 at the University of California, Berkeley. *Sp140$^{-/-}$* mice were previously generated by the
385 Vance Lab [35].

386 Pet shop co-housed mice

387 6-week-old female C57BL/6 mice were purchased from Jackson Laboratories and
388 housed in Innovivo IVC Rat Cages. 8 C57BL/6 mice were housed per cage. Each group
389 was co-housed with one female pet shop mouse purchased from the East Bay Vivarium
390 (Berkeley, CA) for 60 days. Upon importation of the pet shop mice, each mouse was
391 tested for serological presence of pathogens by Vrl Animal Health Diagnostics. Mice
392 were weighed every 3-7 days and monitored for weight loss.

393 Bacterial strains

394 Mtb strain Erdman was a gift from Sarah Stanley at University of California, Berkeley.
395 Mtb expressing Wasabi or mCherry were generated as previously described[75].
396 *Legionella pneumophila* strains were JR32 and isogenic mutants that were produced as
397 previously described[41]. Lp expressing mCherry was produced and cultured as
398 previously described[23]. The mCherry expressing plasmid was a gift from Sunny
399 Shin[76]. All infections were performed with strains lacking *flaA.*

400 Mtb infections

401 For standard low-dose infections, a previously frozen aliquot of Mtb was diluted in 20
402 mL of distilled water. 9 mL of the diluted culture was loaded into the nebulizer of an
403 inhalation exposure system (Glas-Col, Terre-Haute, IN) to deliver ~10-50 CFU of
404 bacteria per mouse as determined by measuring CFU in the lungs 1 day post-infection.
405 For ultra-low dose infections, the infectious dose was first estimated by calculating the
406 volume needed to deliver 1 CFU based on the volume needed to achieve an infectious
407 dose of 20 CFUs in previous experiments. The frozen stock was serially diluted, and the
408 appropriate volume was added to 20 mL of distilled water. The ultra-low infectious dose
409 was confirmed by calculating the percent of infected mice per experiment instead of

410 measuring CFU in the lungs at 1 day post-infection[38]. To enumerate CFU at 1 day
411 post-infection, lungs were homogenized in 1 mL of PBS containing 0.05% Tween-80
412 (PBS-T) and the entirety of the lung was across 4 plates. For other time points, 100 µL
413 were taken from suspensions from lungs either collected in 1 mL of PBS-T or from the 5
414 mL RMPI solution used for flow cytometry sample collection. Samples were then serially
415 diluted in PBS containing 0.05% Tween-80. Serial dilutions were plated on 7H11 plates
416 supplemented with 0.5% glycerol and BBL Middlebrook OADC Enrichment media (BD
417 Biosciences). Colonies were counted after 3 weeks incubation at 37°C.

418 Lp infections

419 For infections, frozen cultures were streaked out onto BCYE plates and incubated at 37°C
420 to obtain single colonies, which were subsequently streaked onto a new BCYE plate and
421 incubated at 37°C to obtain a 1 cm by 1 cm bacterial patch. The patch was then collected
422 and grown for ~20 hours in CYE media with streptomycin (100 µg/mL). The optical density
423 was measured at 600 nm. The culture was diluted to 2.5 x 10^6 CFU/mL in sterile PBS.
424 The mice were anesthetized with ketamine and xylazine by intraperitoneal injection the
425 infected intranasally with 40 µL with PBS to deliver 1 x 10^5 CFU per mouse. The infectious
426 dose was confirmed by measuring CFU in the lungs 4 hours post-infection. Lungs were
427 harvested in either 5 mL of sterile water at the 4 hour time point or 1 mL of sterile water
428 at all other time points. Samples were then serially diluted in water and plated on BCYE
429 plates.

430 Flow cytometry

431 For flow cytometry, mouse lungs were harvested at 14 days post-Mtb-infection. The
432 entire lung was harvested into a gentleMACS C tube (Miltenyi Biotec) containing 3 mL

433 of RPMI media with 70 µg/mL of Liberase TM (Roche) and 30 µg/mL of Dnase I
434 (Roche). Lungs were processed with the lung_01 setting on the gentleMACS (Miltenyi
435 Biotec) and incubated at 37°C for 30 minutes. To obtain a single cell suspension, the
436 samples were then homogenized on lung_02 setting on the gentleMACS. 2 mL of
437 phosphate-buffered saline (PBS) containing 20% Newborn Calf Serum (Thermo Fisher
438 Scientific) was then added to quench the digestion. Samples were then filtered through
439 70 µM SmartStrainers (Miltenyi Biotec). The single cell suspension was then spun down
440 and resuspended in 500 µL of PBS containing 5% Newborn Calf Serum and 0.05%
441 sodium azide. 100 uL were then stained with antibodies for 30 minutes at room
442 temperature with the following antibodies: BV421-labeled PD-L1 (HIH5, BD
443 Biosciences), BV480-labeled B220 (RA3-6B2, BD Biosciences), CD90.2-labeled (53-
444 2.1, BD Biosciences), SB645-labeled MHC Class II (I-A/I-E) (M5/114.15.2, Thermo
445 Fisher Scientific), BV786-labeled Ly-6C (HK1.4, BioLegend), PE-labeled MerTK
446 (DS5MMER, Thermo Fisher Scientific), APC-labeled CD64 (X54-5/7.1, BioLegend),
447 APC-R700-labeled Siglec-F (E50-2440, BD Biosciences), APC/Fire 750-labeled Ly-6G
448 (1A8, BioLegend), BUV396-labeled CD11b (M1/70, BD Biosciences), BUV496-labeled
449 CD45 (30-F11, BD Biosciences), BUV737-labeled CD11c (HL3, BD Biosciences), and
450 BV-785-labeld CD86 (GL-1, BioLegend). All staining cocktails contained True-Stain
451 monocyte blocker (BioLegend), Super Bright Complete Staining Buffer (Thermo Fisher
452 Scientific), and GhostDye 510 (Tonbo). Samples were then fixed for 30 minutes with
453 Cytofix/Cytoperm (BD Biosciences) before removal from the BSL3. Cell numbers were
454 calculated by adding CountBright Plus Absolute Counting Beads (Invitrogen) to each
455 sample. Samples were analyzed on a LSRFortessa X-20 (BD Biosciences) or an Aurora

456 (Cytek) cytometer. Data were analyzed using Flowjo Version 10 (BD Biosciences).
457 Gating was performed as previously described[75].

458 Sorting Immune Cells for scRNA-seq

459 3 C57BL/6 mice were infected with 10^5 CFU of Lp-*ΔflaA* expressing an mCherry
460 plasmid. After 3 days, these mice, along with 3 other naïve C57BL/6 mice, were
461 subsequently infected with ~50 CFU of Mtb-mCherry. At 14 days post-infection, the
462 lungs were harvested and processed as for flow cytometry, as described above.
463 Samples were then stained on ice for 30 minutes with APC-labeled CD64 (X54-5/7.1,
464 BioLegend). Myeloid cells were magnetically enriched using an EasySep APC Positive
465 Selection Kit II (StemCell Technologies) and MojoSort Magnets (BioLegend). Samples
466 were then stained on ice for 45 minutes with the following anti-mouse antibodies in the
467 presence of True-Stain Monocyte Blocker (BioLegend): TruStain FcX PLUS (S17011E,
468 BioLegend), BV786-labeled CD45.2 (104, BioLegend), and Pacific Blue-labeled B220
469 (RA3-6B2, BioLegend), CD90.2 (53-2.1, BioLegend), and Ly6G (1A8, BioLegend). The
470 Pacific Blue-labeled antibodies were used to exclude neutrophils, T cells, and B cells.
471 Additionally, the following TotalSeq-A-labeled anti-mouse antibodies were added to
472 detect protein expression in the scRNA-seq dataset: Ly6C (HK1.4, BioLegend), CD274
473 (MIH6, BioLegend), Siglec F (S17007L, BioLegend), CSF1R (AFS98, BioLegend),
474 CD11b (M1/70, BioLegend), CD86 (GL-1, BioLegend), and MHC II (M5/114.15.2,
475 BioLegend). A unique anti-mouse TotalSeq-A Hashtag antibody (1-6; BioLegend) was
476 added to each sample to allow up to 6 samples to be mixed per lane on the 10X
477 Chromium Next GEM Chip (10X Genomics). After staining, cells were resuspended in
478 PBS with 5% Newborn Calf Serum and Sytox Blue Dead Cell Stain (Thermo Fisher
479 Scientific). Cells were sorted using a 120 μm microfluidic sorting chip in a 4 laser SH-

480 800 cell sorter (Sony) on the purity setting. Cells were collected in PBS containing 50%
481 fetal calf serum.
482
483 scRNA-seq library generation and sequencing

484 Single-cell RNA-sequencing was preformed following previously published
485 protocols[75]. Briefly, the v3.1 chemistry Chromium Single Cell 3' Reagent Kit (10X
486 Genomics) was used to generate scRNA-seq libraries. The manufacturer protocol was
487 followed, with the following minor modifications. Lanes of the 10X Chromium Next GEM
488 Chip were super-loaded with 29,000 cells. During the loading step, 0.5 U/µL RNaseOUT
489 Recombinant Ribonuclease Inhibitor (Invitrogen) was added to single cell RT master
490 mix. During the cDNA amplification, 1 µL of ADT and HTO additive primers (0.2 µM
491 stock) were added as recommended by the CITE-seq and Cell Hashing Protocol[42].
492 After the purification step, samples were decontaminated by 2 rounds of centrifugation
493 through a 0.2 µM filter microcentrifuge tubes and removed from the BSL3. cDNA
494 libraries were prepared following the 10X Genomics protocol. The ADT and HTO
495 libraries were prepared following the CITE-Seq and Cell Hashing Protocols. DNA quality
496 was measured using a TapeStation (Agilent). The cDNA, ADT and HTO libraries were
497 pooled at the following proportion: 80% cDNA, 10% ADT, and 10% HTO. The libraries
498 were sequenced on an Illumina platform (Azenta).

499 ScRNA-seq data processing

500 Raw reads were processed into count matrices with CellRanger v8.0.0 (10x Genomics).
501 The matrices were analyzed in R (RStudio) using Seurat v5.1.0. Cells were filtered to
502 retain singlets expressing 200–4,500 genes with <5% mitochondrial reads. RNA data

were normalized with NormalizeData and subsequently transformed with SCTransform while regressing out mitochondrial content. Principal component analysis (PCA) and UMAP were performed using the top 30 dimensions, and nearest-neighbor graphs were built on the same dimensions. ADT features were set as variable, normalized using centered log-ratio transformation with a margin of 2, scaled, and reduced by PCA using three principal components. Multi-modal integration was performed using FindMultiModalNeighbors, combining five RNA dimensions and three ADT dimensions. UMAP was then computed using weighted nearest-neighbor graphs, and clustering was performed with FindClusters (algorithm = 3; resolution = 0.3). Data visualization was performed with tidyverse, EnhancedVolcano, and Seurat plotting functions.

Acknowledgements

We thank members of the Vance, Barton, Stanley, and Cox labs for advice and discussion. We also thank Jesse Rodriguez, Joceline Morales, the East Bay Vivarium, and the Office of Laboratory Animal Care for assistance with mice. MRF was supported by a Sidney Mac Donald Russell Family fellowship from the UC Berkeley Center for Emerging and Neglected Diseases. Research in the laboratory of REV is funded by an Investigator Award from the Howard Hughes Medical Institute and by NIH grants AI066302, AI075039, and AI155634.

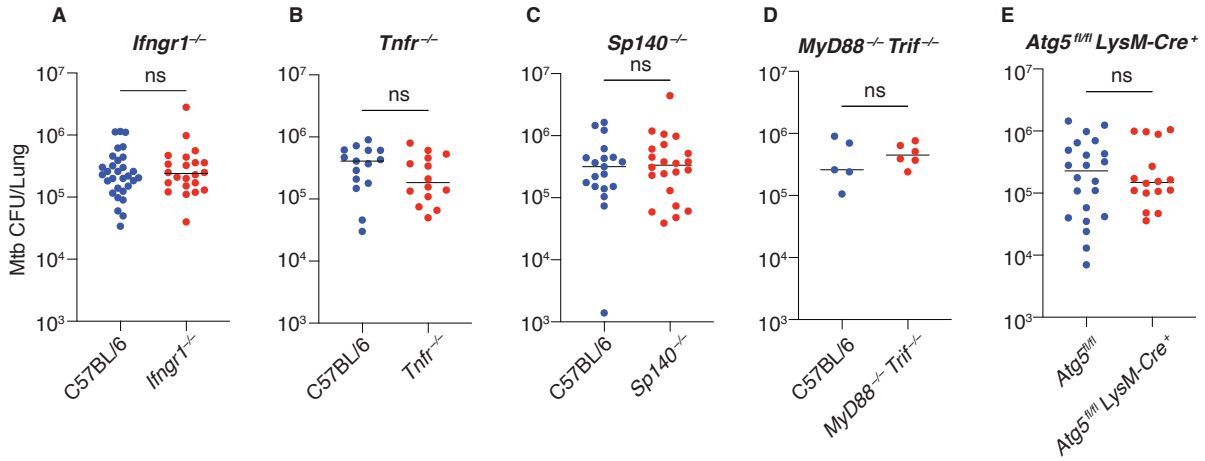

522

523 **Figure 1. Innate immune knockout mice are not more susceptible to Mtb than**

524 **wildtype**

525 (A-E) Colony forming units (CFUs) of Mtb in the lungs of wildtype C57BL/6 and (A)

526 *Ifngr1*$^{-/-}$ (B) *Tnfr*$^{-/-}$ (C) *Sp140*$^{-/-}$ (D) *MyD88*$^{-/-}$*Trif*$^{-/-}$ or (E) *Atg5*$^{fl/fl}$ and *Atg5*$^{fl/fl}$ *LysM-Cre*$^{+}$.

527 Lungs were analyzed 14 days post infection. The bars represent the median where CFU

528 was detected. Pooled data from one to three independent experiments are shown. A

529 Mann-Whitney test was used to calculate significance. *$p < 0.05$

	Wild-type mice			Knockout mice					
	Infected mice	Uninfected mice	Percent infected	Infected mice	Uninfected mice	Percent infected	Chi-square test with Yate's correction	*df*	*p*
***Ifngr1*$^{-/-}$ *vs* wild-type**	30	8	78.9%	22	16	57.9%	2.984	1	0.0841
***Tnfr*$^{-/-}$ *vs* wild-type**	15	6	71.4%	14	15	48.2	1.1814	1	0.178
***Sp140*$^{-/-}$ *vs* wild-type**	14	23	37.8%	15	19	44.1%	0.088	1	0.7971
***MyD88*$^{-/-}$*Trif*$^{-/-}$ *vs* wild-type**	5	5	50.0%	6	4	60.0%	0.202	1	0.6531
***Atg5*$^{fl/fl}$ *LysM*^{Cre} *vs* wild-type**	22	14	61.1%	16	17	48.5%	0.657	1	0.4174

Table 1. Calculation of the fraction of infected mice after ULD aerosol infection

Percent of infected wild-type or knockout mice and the results of chi-square tests with Yate's correction of CFU positive and CFU negative wild-type or innate immune deficient mice infected with an ultra-low dose of Mtb. A 2x2 contingency table with used to calculate the results of the chi-square test.

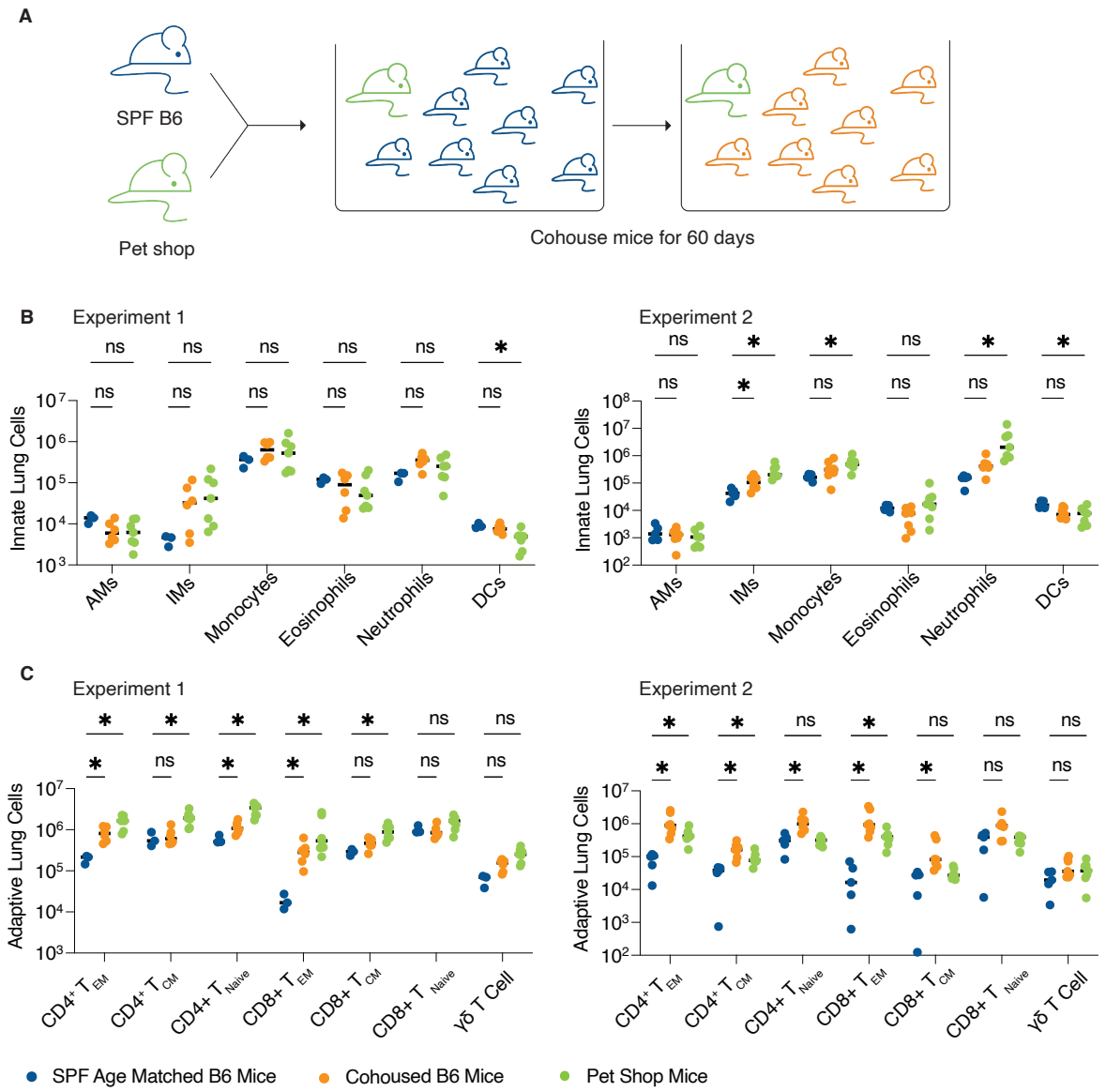

536

537 **Figure 2. C57BL/6 mouse immune system can be primed by cohousing with pet**

538 **shop mice.**

539 (A) Schematic of cohousing set up. Female C57BL/6 mice were cohoused with adult

540 female pet shop mice for 60 days, during which co-housed mice are exposed to

541 pathogenic, commensal, and opportunistic microbes carried by pet shop mice.

542 (B-C) Lung innate (B) and adaptive (C) immune cells were profiled from age-matched

543 SPF C57BL/6 mice, cohoused C57BL/6 mice, or pet shop mice in two independent

experiments. A One-way ANOVA on log_{10}-transformed data, followed by pairwise comparisons using Tukey's test was performed to determine significance. EM= Effector memory, CM = Central memory, $*p \leq 0.05$

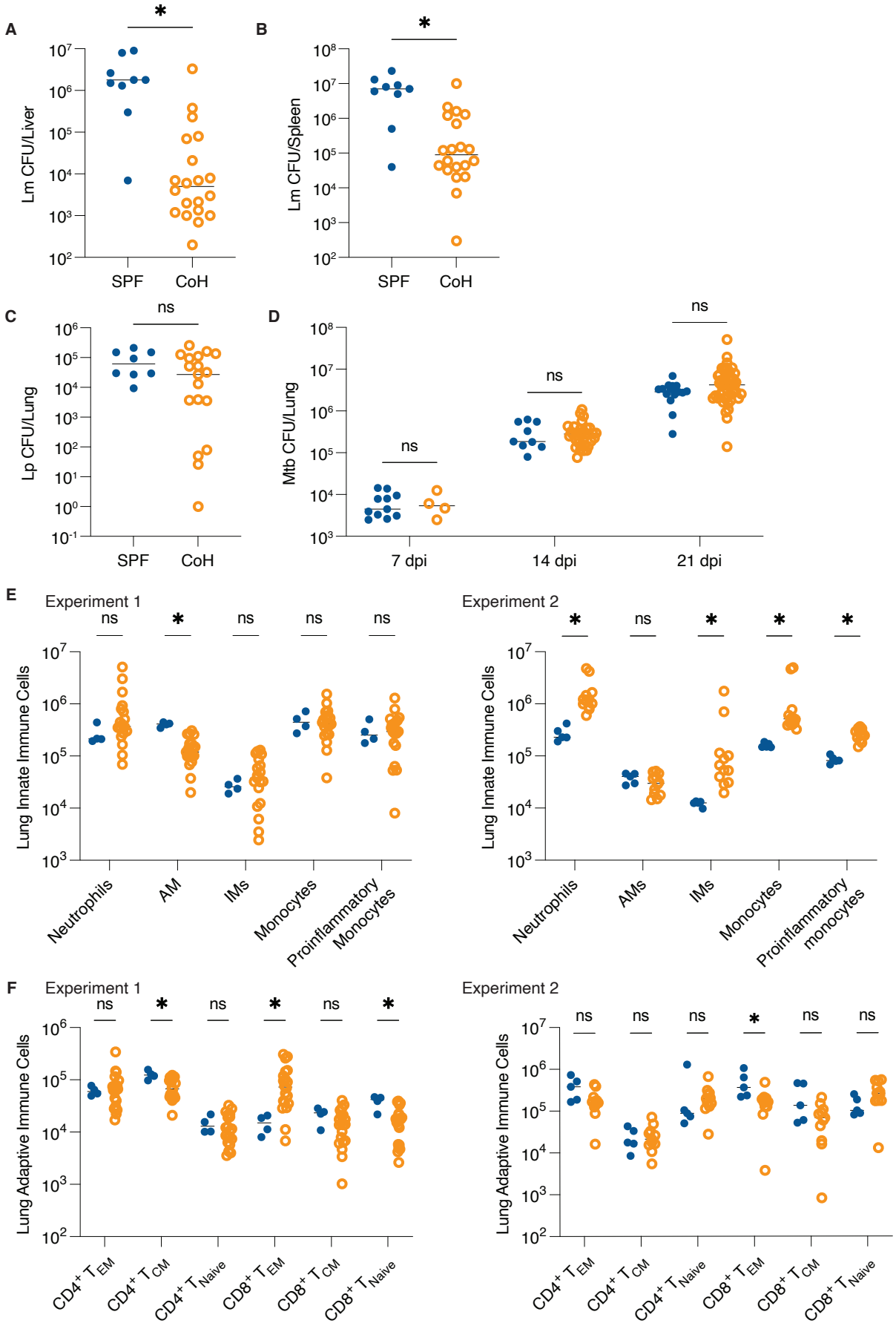
A
Lm CFU/Liver
SPF
CoH
B
Lm CFU/Spleen
C
Lp CFU/Lung
D
Mtb CFU/Lung
7 dpi
14 dpi
21 dpi
ns
E
Experiment 1
Experiment 2
Lung Innate Immune Cells
Neutrophils
AM
IMs
Monocytes
Proinflammatory Monocytes
AMs
F
Lung Adaptive Immune Cells
CD4+ TEM
CD4+ TCM
CD4+ TNaive
CD8+ TEM
CD8+ TCM
CD8+ TNaive

548

549 **Figure 3. Pet shop cohoused mice exhibit enhanced control of Lm but not Mtb**

550 (A-B) *Listeria monocytogenes* (Lm) CFUs from the liver (A) and spleen (B) from either co-
551 housed (CoH) C57BL/6 mice or age-matched SPF controls.

552 (C) Lp CFUs from the lung of either co-housed C57BL/6 mice or age-matched SPF
553 controls.

554 (D) Mtb CFUs from the lung of either co-housed C57BL/6 mice or age-matched SPF
555 controls.

556 (E) Quantification of innate lung cell populations from co-housed and SPF age matched
557 mice from two independent cohousing experiments.

558 (F) Quantification of adaptive lung cell populations from co-housed and SPF age
559 matched mice from two independent co-housing experiments.

560 The bars represent the median values. Multiple Mann-Whitney tests were used to
561 calculate significance. $*p \leq 0.05$

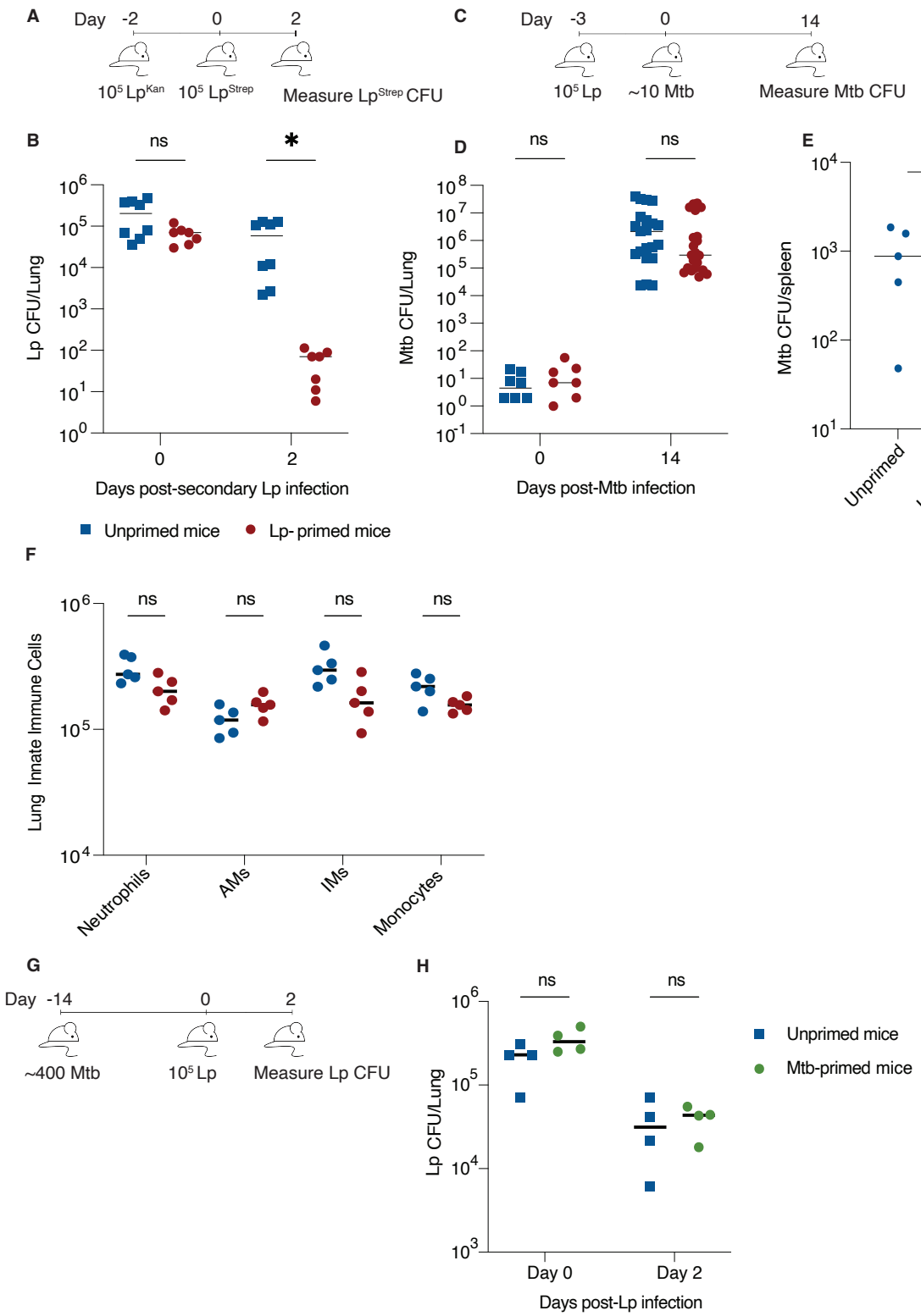

562

563 **Figure 4. Priming with Lp does not curb Mtb replication**

564 (A) Schematic of Lp co-infection. Mice were infected with Lp containing a kanamycin
565 resistance gene (Lp^{Kan}) or were left uninfected. Two days later, all mice were infected
566 with Lp containing a streptomycin resistance gene (Lp^{Strep}). Two days later, Lp^{Strep} CFUs
567 were measured.
568 (B) Lp lung CFU from unprimed mice or mice primed with a previous infection of
569 Lp. Results shown are from 2 combined experiments.
570 (C) Schematic of Lp/Mtb co-infection. Mice were infected with Lp or were left uninfected.
571 Three days later, all mice were infected with Mtb. 14 days later, Mtb CFU was
572 measured in the lung and spleen and samples taken for flow cytometry analysis.
573 (D) Lung Mtb CFU from unprimed or mice primed with a previous infection of
574 Lp. Results shown are from 3 combined experiments.
575 (E) Spleen Mtb CFU from unprimed or mice primed with a previous infection of Lp.
576 (F) Lung innate immune cells from unprimed mice or Lp-primed mice.
577 (G) Schematic of Mtb/Lp co-infection. Mice were infected with ~400 CFU of Mtb or were
578 left uninfected. 14 days later, all mice were infected with Lp.
579 (H) Lp lung CFU from unprimed mice or mice primed with a previous infection of Mtb.
580 The bars represent the median where CFU was detected. Mann-Whitney tests were
581 used to calculate significance. $*p \leq 0.05$

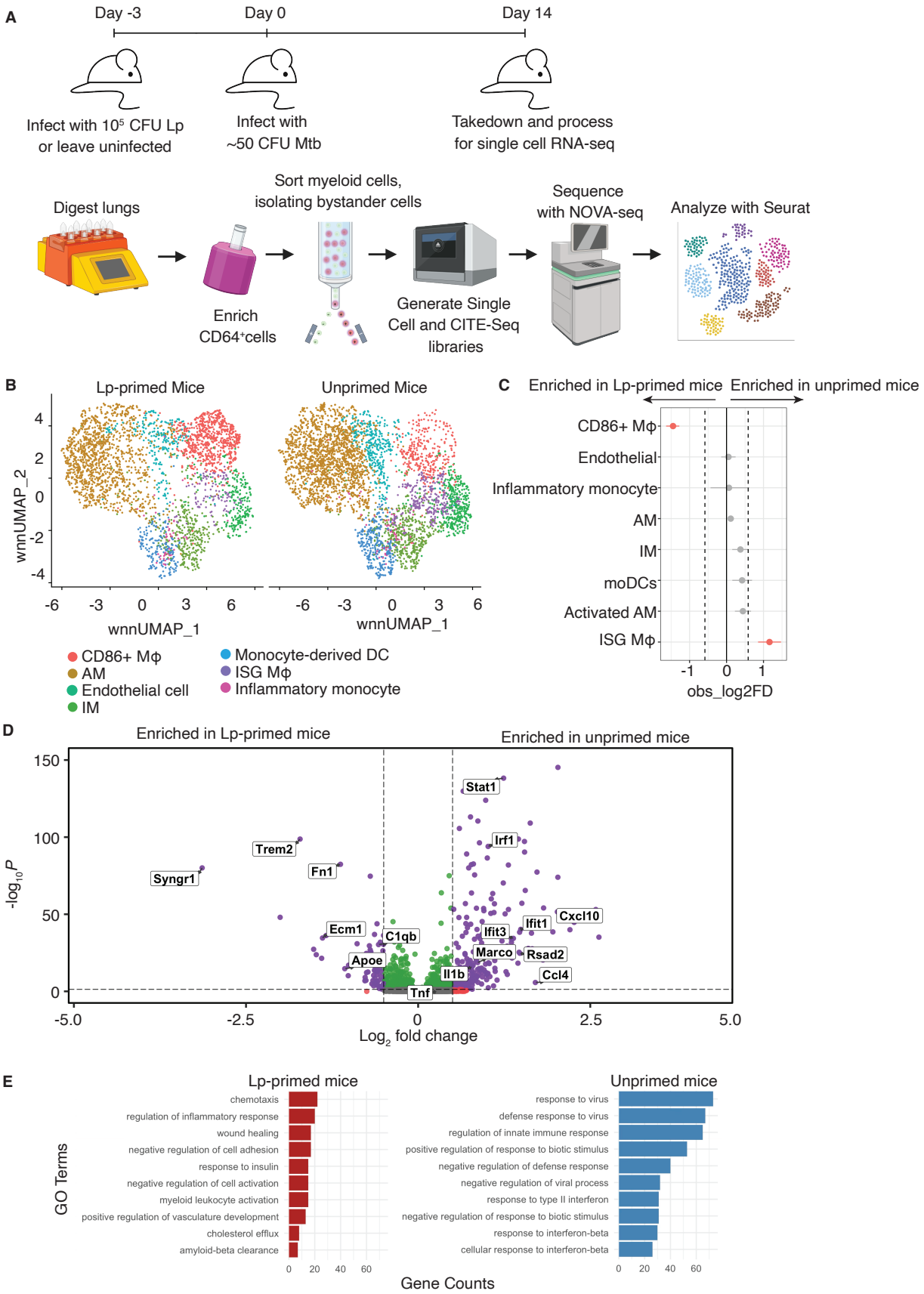
A
Day -3
Day 0
Day 14
Infect with 10⁵ CFU Lp or leave uninfected
Infect with ~50 CFU Mtb
Takedown and process for single cell RNA-seq
Digest lungs
Enrich CD64⁺cells
Sort myeloid cells, isolating bystander cells
Generate Single Cell and CITE-Seq libraries
Sequence with NOVA-seq
Analyze with Seurat
B
Lp-primed Mice
Unprimed Mice
wnnUMAP_2
wnnUMAP_1
CD86+ Mϕ
AM
Endothelial cell
IM
Monocyte-derived DC
ISG Mϕ
Inflammatory monocyte
C
Enriched in Lp-primed mice
Enriched in unprimed mice
CD86+ Mϕ
Endothelial
Inflammatory monocyte
AM
IM
moDCs
Activated AM
ISG Mϕ
obs_log2FD
D
Enriched in Lp-primed mice
Enriched in unprimed mice
-log10P
Log2 fold change
Stat1
Irf1
Trem2
Fn1
Syngr1
Ecm1
C1qb
Apoe
Ifit3
Ifit1
Cxcl10
Marco
Rsad2
Il1b
Ccl4
Tnf
E
Lp-primed mice
Unprimed mice
GO Terms
chemotaxis
regulation of inflammatory response
wound healing
negative regulation of cell adhesion
response to insulin
negative regulation of cell activation
myeloid leukocyte activation
positive regulation of vasculature development
cholesterol efflux
amyloid-beta clearance
response to virus
defense response to virus
regulation of innate immune response
positive regulation of response to biotic stimulus
negative regulation of defense response
negative regulation of viral process
response to type II interferon
negative regulation of response to biotic stimulus
response to interferon-beta
cellular response to interferon-beta
Gene Counts

582

583 **Figure 5. Lp priming alters gene expression and cell types in the lung after Mtb**
584 **infection**

585 (A) Model of the processing steps involved in generating the scRNA-seq dataset

586 (B) UMAP of unbiased clusters of myeloid cells in either unprimed or Lp-primed mice
587 infected with Mtb. Only bystander cells are displayed. Lungs were analyzed 14 days
588 post Mtb-mCherry infection.

589 (C) Relative differences in cell proportions for each cluster between unprimed and Lp-
590 primed samples. Clusters colored red had an FDR < 0.05 and mean | Log2 fold
591 enrichment | > 0.58 compared to the normal colon (permutation test; n=10,000).

592 (D) Differential gene expression (DEG) of bystander myeloid cells from Lp-primed or
593 unprimed mice infected with Mtb.

594 (E) DEGs were analyzed for gene functional annotations of GO terms.

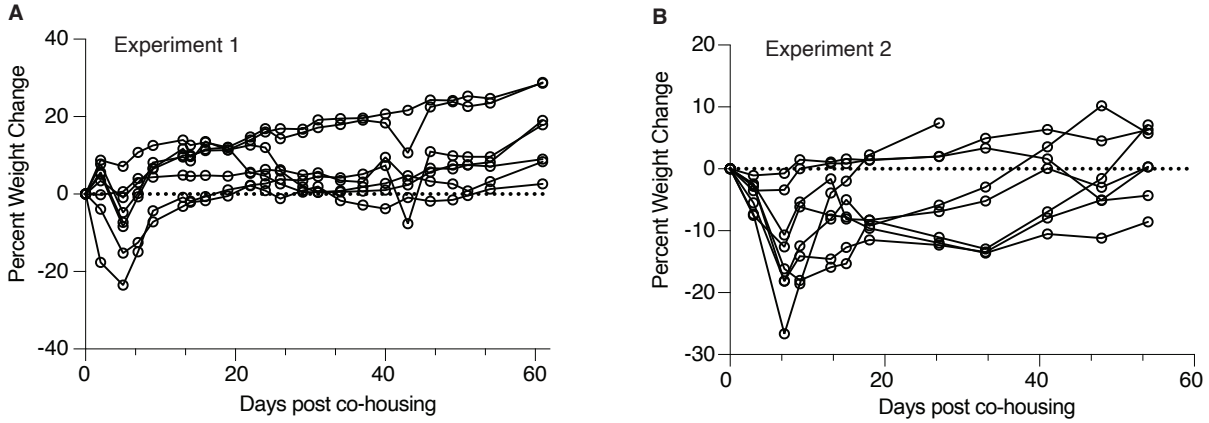

Supplemental Figure 1. Weight changes in co-housed mice

(A-B) Average percent weight change of C57BL/6 mice cohoused with pet shop mice in two individual experiments. Each line represents the average weight change of up to 8 mice in one cage. Mice were weighed every 3-7 days over 60 days.

600

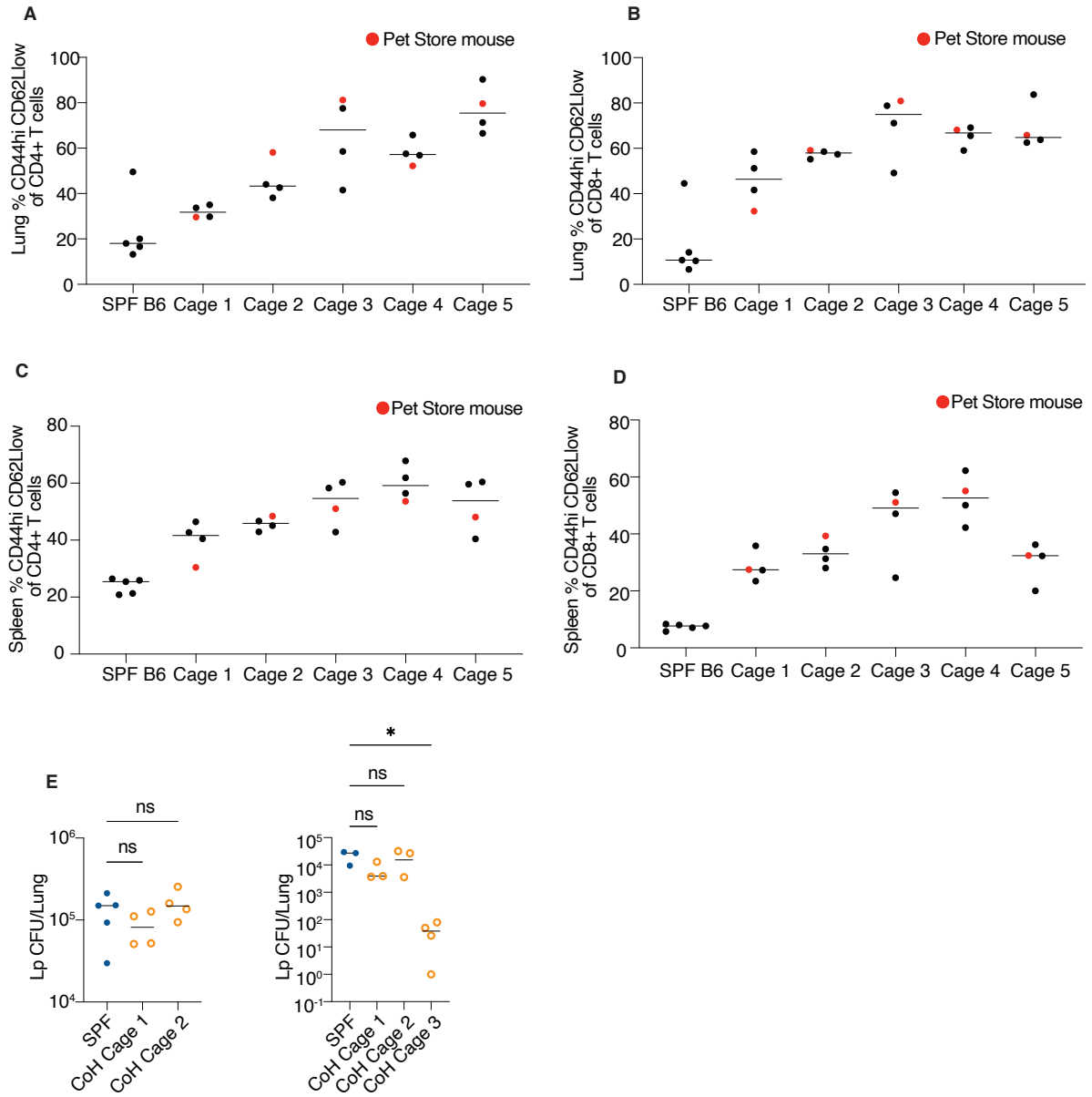

601

602 **Supplemental Figure 2. The founder pet shop mouse influences cell counts and**

603 **infection outcomes in cohoused C57BL/6 mice**

604 (A-B) Percent of $CD4^+$ (A) or $CD8^+$ (B) T effector memory cells in the lungs of either

605 SPF C57BL/6 mice, pet shop cohoused, or pet shop mice (red).

606 (C-D) % of $CD4^+$ (C) or $CD8^+$ (D) T effector memory cells in the spleens of either SPF

607 C57BL/6 mice, pet shop cohoused, or pet shop mice (red).

608 (E) Lp lung CFU from two separate experiments at 2 days post infection. The bars

609 represent the median where CFU was detected. Mann-Whitney tests were used to

610 calculate significance. $*p < 0.05$

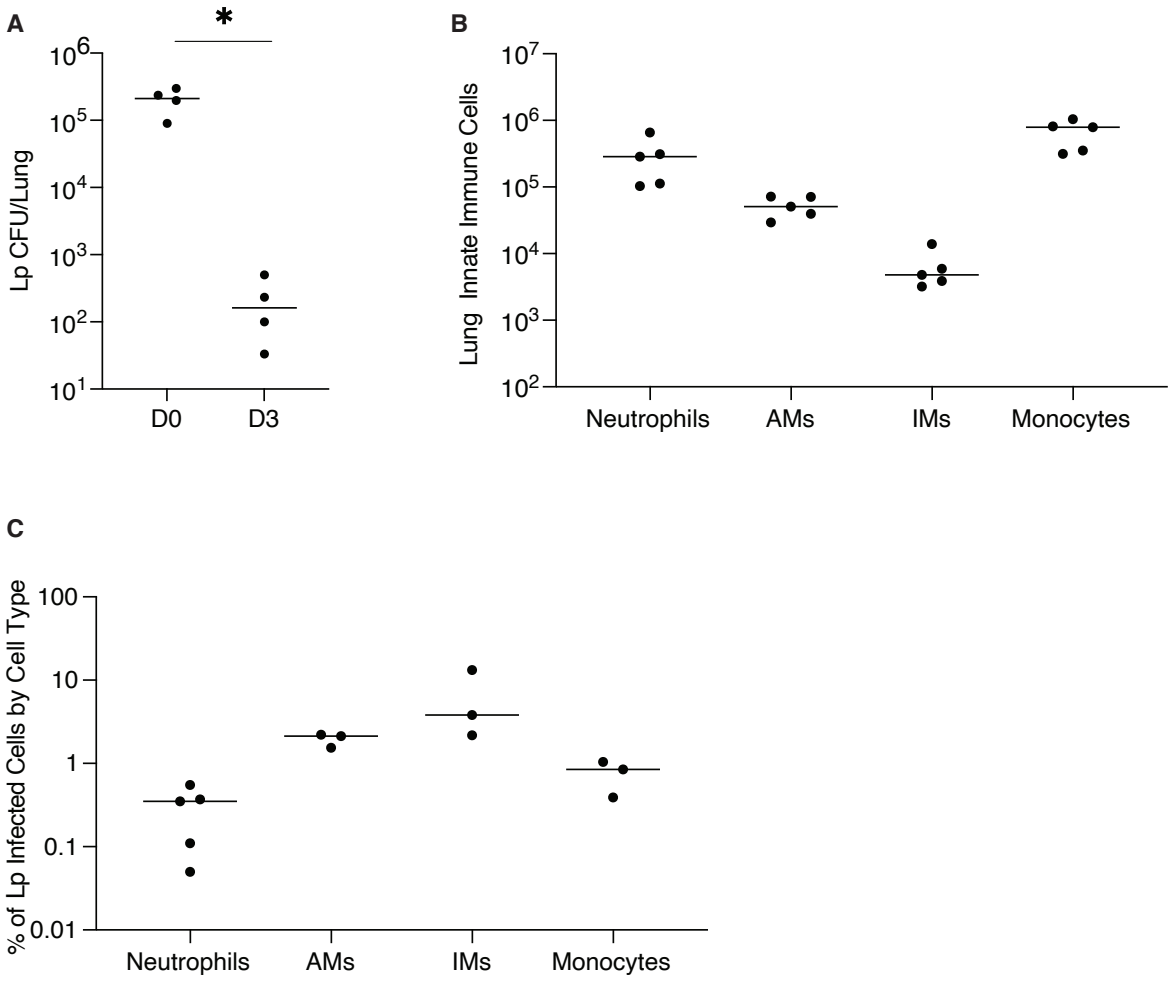

Supplemental Figure 3. Characterizing Lp infection in C57BL/6 mice

(A) Lp Lung CFU measured 4 hours post infection (D0) and 3 days post-infection (D3).

(B) Lung innate immune cells 1 day post-Lp infection.

(C) Localization of Lp as measured by the detection of fluorescent bacteria as a percent of each cell type.

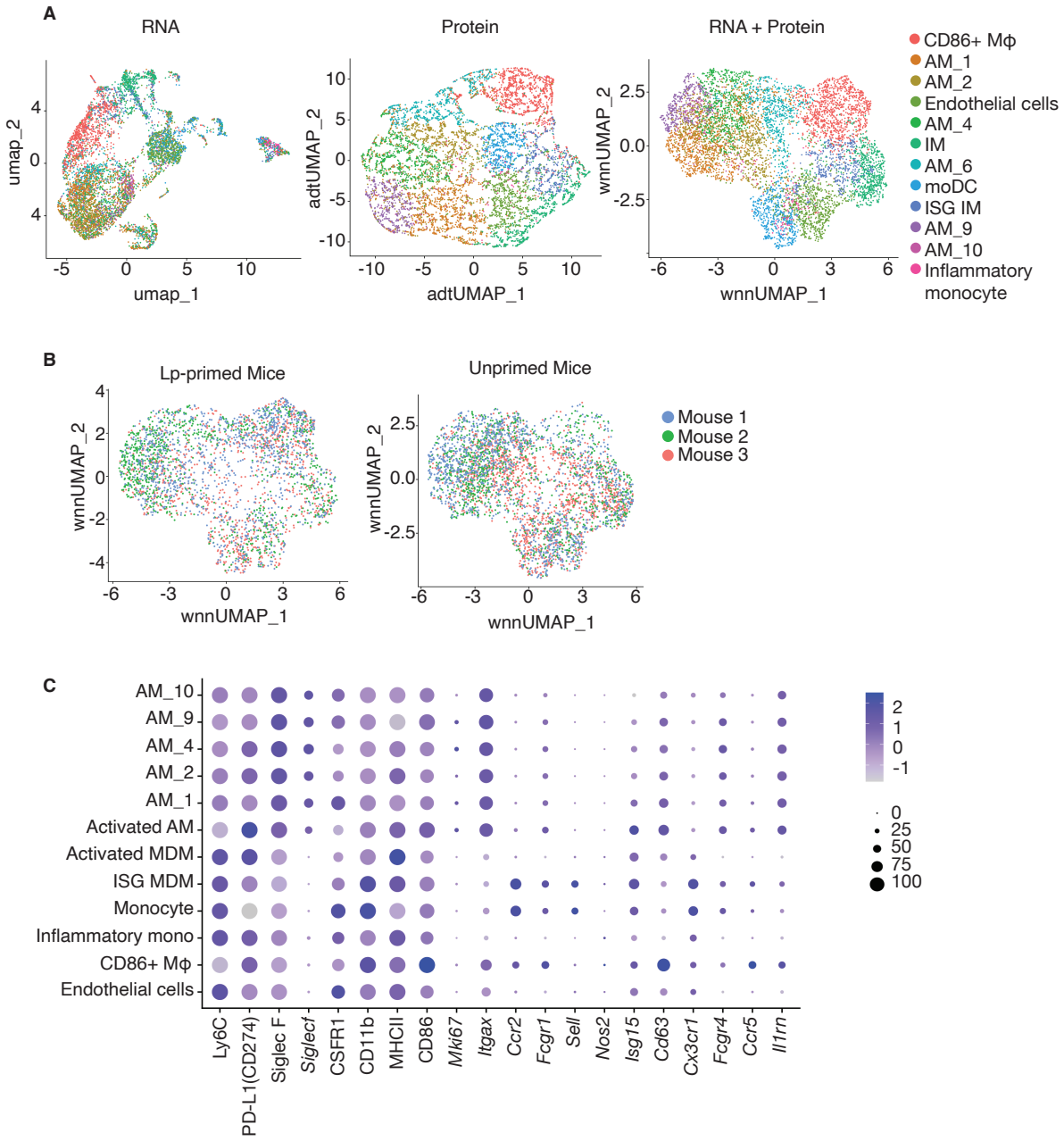

Supplemental Figure 4. Identification of lung myeloid cells from scRNA-seq.

(A) UMAP plots showing cell clustering of combined mRNA and protein expression, mRNA expression, or protein expression. Only bystander cells are shown.

(B) UMAP plots showing cell clustering of biological replicates of unprimed or Lp-primed mice. Only bystander cells are shown.

623 (C) Protein and mRNA expression of lineage-defining myeloid cell markers used for
624 cluster classification. Both unprimed and Lp-primed mice were analyzed to identify
625 clusters.

		Experiment 1			Experiment 2		
Agents Tested	Methodology	Tested	Positive	Negative	Tested	Positive	Negative
Mouse parvovirus	SEROLOGY	7	3	4	7	2	5
Minute virus of mice	SEROLOGY	7	0	7	7	4	3
Parvo NS-1	SEROLOGY	7	4	3	7	3	4
Mouse hepatitis virus	SEROLOGY	7	6	1	7	7	0
Murine norovirus	SEROLOGY	7	2	5	7	3	4
Theilovirus (GD7TMEV)	SEROLOGY	7	0	7	7	0	7
Rotavirus	SEROLOGY	7	0	7	7	3	4
Sendai virus	SEROLOGY	7	0	7	7	0	7
Pneumonia virus	SEROLOGY	7	0	7	7	2	5
Reovirus 1,2,3	SEROLOGY	7	0	7	7	0	7
Lymphocytic choriomeningitis virus	SEROLOGY	7	0	7	7	0	7
Mouse adenovirus 1	SEROLOGY	7	0	7	7	0	7
Mouse adenovirus 2	SEROLOGY	7	0	7	7	0	7
Ectromelia virus	SEROLOGY	7	0	7	7	0	7
Polyoma virus	SEROLOGY	7	0	7	7	0	7
Murine cytomegalovirus	IFA	7	0	7	7	0	7
CAR Bacillus	SEROLOGY	7	0	7	7	0	7
Mouse thymic virus	IFA	7	0	7	7	0	7

Supplemental Table 1. Pathogen diagnostic panel of pet shop mice

Pathogen diagnostic panel performed on blood samples of pet shop mice by serology or immunofluorescence assay (IFA) over two independent experiments. 7 mice were tested for each experiment.

632 **References**

633 1. Ravesloot-Chávez MM, Van Dis E, Stanley SA. The Innate Immune Response to
634 Mycobacterium tuberculosis. Annu Rev Immunol. 2021;39:611-37. Epub 20210226. doi:
635 10.1146/annurev-immunol-093019-010426. PubMed PMID: 33637017.
636 2. Cohen SB, Gern BH, Delahaye JL, Adams KN, Plumlee CR, Winkler JK, et al. Alveolar
637 Macrophages Provide an Early Mycobacterium tuberculosis Niche and Initiate
638 Dissemination. Cell Host Microbe. 2018;24(3):439-46.e4. Epub 20180823. doi:
639 10.1016/j.chom.2018.08.001. PubMed PMID: 30146391; PubMed Central PMCID:
640 PMC6152889.
641 3. Rothchild AC, Olson GS, Nemeth J, Amon LM, Mai D, Gold ES, et al. Alveolar
642 macrophages generate a noncanonical NRF2-driven transcriptional response to
643 Mycobacterium tuberculosis in vivo. Sci Immunol. 2019;4(37). doi:
644 10.1126/sciimmunol.aaw6693. PubMed PMID: 31350281; PubMed Central PMCID:
645 PMC6910245.
646 4. Pisu D, Johnston L, Mattila JT, Russell DG. The frequency of CD38+ alveolar
647 macrophages correlates with early control of M. tuberculosis in the murine lung. Nat
648 Commun. 2024;15(1):8522. Epub 20241002. doi: 10.1038/s41467-024-52846-w. PubMed
649 PMID: 39358361; PubMed Central PMCID: PMC11447019.
650 5. Pisu D, Huang L, Narang V, Theriault M, Lê-Bury G, Lee B, et al. Single cell analysis of
651 M. tuberculosis phenotype and macrophage lineages in the infected lung. J Exp Med.
652 2021;218(9). Epub 20210722. doi: 10.1084/jem.20210615. PubMed PMID: 34292313;
653 PubMed Central PMCID: PMC8302446.
654 6. Mai D, Jahn A, Murray T, Morikubo M, Lim PN, Cervantes MM, et al. Exposure to
655 Mycobacterium remodels alveolar macrophages and the early innate response to
656 Mycobacterium tuberculosis infection. PLoS Pathog. 2024;20(1):e1011871. Epub
657 20240118. doi: 10.1371/journal.ppat.1011871. PubMed PMID: 38236787; PubMed Central
658 PMCID: PMC10796046.
659 7. Mata E, Tarancon R, Guerrero C, Moreo E, Moreau F, Uranga S, et al. Pulmonary BCG
660 induces lung-resident macrophage activation and confers long-term protection against
661 tuberculosis. Sci Immunol. 2021;6(63):eabc2934. Epub 20210924. doi:
662 10.1126/sciimmunol.abc2934. PubMed PMID: 34559551.
663 8. Wolf AJ, Desvignes L, Linas B, Banaiee N, Tamura T, Takatsu K, et al. Initiation of the
664 adaptive immune response to Mycobacterium tuberculosis depends on antigen production
665 in the local lymph node, not the lungs. The Journal of experimental medicine.
666 2008;*205*:105–15. doi: https://doi.org/10.1084/jem.20071367.
667 9. Scanga CA, Bafica A, Feng CG, Cheever AW, Hieny S, Sher A. MyD88-deficient mice
668 display a profound loss in resistance to Mycobacterium tuberculosis associated with
669 partially impaired Th1 cytokine and nitric oxide synthase 2 expression. Infect Immun.
670 2004;72(4):2400-4. doi: 10.1128/IAI.72.4.2400-2404.2004. PubMed PMID: 15039368;
671 PubMed Central PMCID: PMC375220.
672 10. Bean AG, Roach DR, Briscoe H, France MP, Korner H, Sedgwick JD, et al. Structural
673 deficiencies in granuloma formation in TNF gene-targeted mice underlie the heightened
674 susceptibility to aerosol Mycobacterium tuberculosis infection, which is not compensated
675 for by lymphotoxin. J Immunol. 1999;162(6):3504-11. PubMed PMID: 10092807.

676 11. Sugawara I, Yamada H, Li C, Mizuno S, Takeuchi O, Akira S. Mycobacterial infection
677 in TLR2 and TLR6 knockout mice. Microbiol Immunol. 2003;47(5):327-36. doi:
678 10.1111/j.1348-0421.2003.tb03404.x. PubMed PMID: 12825894.
679 12. Bafica A, Scanga CA, Feng CG, Leifer C, Cheever A, Sher A. TLR9 regulates Th1
680 responses and cooperates with TLR2 in mediating optimal resistance to Mycobacterium
681 tuberculosis. J Exp Med. 2005;202(12):1715-24. doi: 10.1084/jem.20051782. PubMed
682 PMID: 16365150; PubMed Central PMCID: PMC2212963.
683 13. Di Paolo NC, Shafiani S, Day T, Papayannopoulou T, Russell DW, Iwakura Y, et al.
684 Interdependence between Interleukin-1 and Tumor Necrosis Factor Regulates TNF-
685 Dependent Control of Mycobacterium tuberculosis Infection. Immunity. 2015;43(6):1125-
686 36. doi: 10.1016/j.immuni.2015.11.016. PubMed PMID: 26682985; PubMed Central PMCID:
687 PMC4685953.
688 14. Kimmey JM, Huynh JP, Weiss LA, Park S, Kambal A, Debnath J, et al. Unique role for
689 ATG5 in neutrophil-mediated immunopathology during M. tuberculosis infection. Nature.
690 2015;528(7583):565-9. Epub 20151209. doi: 10.1038/nature16451. PubMed PMID:
691 26649827; PubMed Central PMCID: PMC4842313.
692 15. Nair S, Huynh JP, Lampropoulou V, Loginicheva E, Esaulova E, Gounder AP, et al. Irg1
693 expression in myeloid cells prevents immunopathology during M. tuberculosis infection. J
694 Exp Med. 2018;215(4):1035-45. Epub 20180306. doi: 10.1084/jem.20180118. PubMed
695 PMID: 29511063; PubMed Central PMCID: PMC5881474.
696 16. Dorhoi A, Desel C, Yeremeev V, Pradl L, Brinkmann V, Mollenkopf HJ, et al. The
697 adaptor molecule CARD9 is essential for tuberculosis control. J Exp Med. 2010;207(4):777-
698 92. Epub 20100329. doi: 10.1084/jem.20090067. PubMed PMID: 20351059; PubMed
699 Central PMCID: PMC2856020.
700 17. MacMicking JD, North RJ, LaCourse R, Mudgett JS, Shah SK, Nathan CF.
701 Identification of nitric oxide synthase as a protective locus against tuberculosis. Proc Natl
702 Acad Sci U S A. 1997;94(10):5243-8. doi: 10.1073/pnas.94.10.5243. PubMed PMID:
703 9144222; PubMed Central PMCID: PMC24663.
704 18. Peignier A, Kim J, Lemenze A, Parker D. Monocyte-regulated interleukin 12
705 production drives clearance of Staphylococcus aureus. PLoS Pathog.
706 2024;20(10):e1012648. Epub 20241017. doi: 10.1371/journal.ppat.1012648. PubMed
707 PMID: 39418302; PubMed Central PMCID: PMC11521269.
708 19. Tsai WC, Strieter RM, Mehrad B, Newstead MW, Zeng X, Standiford TJ. CXC
709 chemokine receptor CXCR2 is essential for protective innate host response in murine
710 Pseudomonas aeruginosa pneumonia. Infect Immun. 2000;68(7):4289-96. doi:
711 10.1128/IAI.68.7.4289-4296.2000. PubMed PMID: 10858247; PubMed Central PMCID:
712 PMC101748.
713 20. Copenhaver AM, Casson CN, Nguyen HT, Fung TC, Duda MM, Roy CR, et al. Alveolar
714 macrophages and neutrophils are the primary reservoirs for Legionella pneumophila and
715 mediate cytosolic surveillance of type IV secretion. Infect Immun. 2014;82(10):4325-36.
716 Epub 20140804. doi: 10.1128/IAI.01891-14. PubMed PMID: 25092908; PubMed Central
717 PMCID: PMC4187856.
718 21. Lettinga KD, Florquin S, Speelman P, van Ketel R, van der Poll T, Verbon A. Toll-like
719 receptor 4 is not involved in host defense against pulmonary Legionella pneumophila

720 infection in a mouse model. J Infect Dis. 2002;186(4):570-3. Epub 20020724. doi:
721 10.1086/341780. PubMed PMID: 12195388.
722 22. Mascarenhas DP, Zamboni DS. Innate immune responses and monocyte-derived
723 phagocyte recruitment in protective immunity to pathogenic bacteria: insights from
724 Legionella pneumophila. Curr Opin Microbiol. 2024;80:102495. Epub 20240621. doi:
725 10.1016/j.mib.2024.102495. PubMed PMID: 38908045.
726 23. Gonçalves AV, Margolis SR, Quirino GFS, Mascarenhas DPA, Rauch I, Nichols RD, et
727 al. Gasdermin-D and Caspase-7 are the key Caspase-1/8 substrates downstream of the
728 NAIP5/NLRC4 inflammasome required for restriction of Legionella pneumophila. PLoS
729 Pathog. 2019;15(6):e1007886. Epub 20190628. doi: 10.1371/journal.ppat.1007886.
730 PubMed PMID: 31251782; PubMed Central PMCID: PMC6622555.
731 24. Plumlee CR, Duffy, F. J., Gern, B. H., Delahaye, J. L., Cohen, S. B., Stoltzfus, C. R.,
732 Rustad, T. R., Hansen, S. G., Axthelm, M. K., Picker, L. J., Aitchison, J. D., Sherman, D. R.,
733 Ganusov, V. V., Gerner, M. Y., Zak, D. E., & Urdahl, K. B. Ultra-low Dose Aerosol Infection of
734 Mice with Mycobacterium tuberculosis More Closely Models Human Tuberculosis. Cell
735 host & microbe. 2021;29(1):68–82. doi: https://doi.org/10.1016/j.chom.2020.10.003.
736 PubMed Central PMCID: PMC7854984.
737 25. Skerrett SJ, Bagby GJ, Schmidt RA, Nelson S. Antibody-mediated depletion of tumor
738 necrosis factor-alpha impairs pulmonary host defenses to Legionella pneumophila. J Infect
739 Dis. 1997;176(4):1019-28. doi: 10.1086/516530. PubMed PMID: 9333161.
740 26. Barry KC, Fontana MF, Portman JL, Dugan AS, Vance RE. IL-1α signaling initiates the
741 inflammatory response to virulent Legionella pneumophila in vivo. J Immunol.
742 2013;190(12):6329-39. Epub 20130517. doi: 10.4049/jimmunol.1300100. PubMed PMID:
743 23686480; PubMed Central PMCID: PMC3682686.
744 27. Blanchard DK, Klein TW, Friedman H, Stewart WE. Kinetics and characterization of
745 interferon production by murine spleen cells stimulated with Legionella pneumophila
746 antigens. Infect Immun. 1985;49(3):719-23. doi: 10.1128/iai.49.3.719-723.1985. PubMed
747 PMID: 2411662; PubMed Central PMCID: PMC261255.
748 28. Martin CJ, Cadena AM, Leung VW, Lin PL, Maiello P, Hicks N, et al. Digitally
749 Barcoding Mycobacterium tuberculosis Reveals In Vivo Infection Dynamics in the
750 Macaque Model of Tuberculosis. mBio. 2017;8(3). Epub 20170509. doi:
751 10.1128/mBio.00312-17. PubMed PMID: 28487426; PubMed Central PMCID: PMC5424202.
752 29. Plumlee CR, Barrett HW, Shao DE, Lien KA, Cross LM, Cohen SB, et al. Assessing
753 vaccine-mediated protection in an ultra-low dose Mycobacterium tuberculosis murine
754 model. PLoS Pathog. 2023;19(11):e1011825. Epub 20231127. doi:
755 10.1371/journal.ppat.1011825. PubMed PMID: 38011264; PubMed Central PMCID:
756 PMC10703413.
757 30. Beura LK, Hamilton SE, Bi K, Schenkel JM, Odumade OA, Casey KA, et al.
758 Normalizing the environment recapitulates adult human immune traits in laboratory mice.
759 Nature. 2016;532(7600):512-6. Epub 20160420. doi: 10.1038/nature17655. PubMed PMID:
760 27096360; PubMed Central PMCID: PMC4871315.
761 31. Huggins MA, Sjaastad FV, Pierson M, Kucaba TA, Swanson W, Staley C, et al.
762 Microbial Exposure Enhances Immunity to Pathogens Recognized by TLR2 but Increases
763 Susceptibility to Cytokine Storm through TLR4 Sensitization. Cell Rep. 2019;28(7):1729-

764 43.e5. doi: 10.1016/j.celrep.2019.07.028. PubMed PMID: 31412243; PubMed Central
765 PMCID: PMC6703181.
766 32. Labuda JC, Fong KD, McSorley SJ. Cohousing with Dirty Mice Increases the
767 Frequency of Memory T Cells and Has Variable Effects on Intracellular Bacterial Infection.
768 Immunohorizons. 2022;6(2):184-90. Epub 20220224. doi:
769 10.4049/immunohorizons.2100069. PubMed PMID: 35210292; PubMed Central PMCID:
770 PMC9624231.
771 33. Flynn JL, Chan J, Triebold KJ, Dalton DK, Stewart TA, Bloom BR. An essential role for
772 interferon gamma in resistance to Mycobacterium tuberculosis infection. J Exp Med.
773 1993;178(6):2249-54. doi: 10.1084/jem.178.6.2249. PubMed PMID: 7504064; PubMed
774 Central PMCID: PMCPMC2191274.
775 34. Flynn JL, Goldstein MM, Chan J, Triebold KJ, Pfeffer K, Lowenstein CJ, et al. Tumor
776 necrosis factor-alpha is required in the protective immune response against
777 Mycobacterium tuberculosis in mice. Immunity. 1995;2(6):561-72. doi: 10.1016/1074-
778 7613(95)90001-2. PubMed PMID: 7540941.
779 35. Ji DX, Witt KC, Kotov DI, Margolis SR, Louie A, Chevée V, et al. Role of the
780 transcriptional regulator SP140 in resistance to bacterial infections via repression of type I
781 interferons. Elife. 2021;10. Epub 20210621. doi: 10.7554/eLife.67290. PubMed PMID:
782 34151776; PubMed Central PMCID: PMC8248984.
783 36. Fremond CM, Yeremeev V, Nicolle DM, Jacobs M, Quesniaux VF, Ryffel B. Fatal
784 Mycobacterium tuberculosis infection despite adaptive immune response in the absence
785 of MyD88. J Clin Invest. 2004;114(12):1790-9. doi: 10.1172/JCI21027. PubMed PMID:
786 15599404; PubMed Central PMCID: PMC535064.
787 37. Watson RO, Bell SL, MacDuff DA, Kimmey JM, Diner EJ, Olivas J, et al. The Cytosolic
788 Sensor cGAS Detects Mycobacterium tuberculosis DNA to Induce Type I Interferons and
789 Activate Autophagy. Cell Host Microbe. 2015;17(6):811-9. Epub 20150602. doi:
790 10.1016/j.chom.2015.05.004. PubMed PMID: 26048136; PubMed Central PMCID:
791 PMCPMC4466081.
792 38. Saini D, Hopkins GW, Seay SA, Chen CJ, Perley CC, Click EM, et al. Ultra-low dose of
793 Mycobacterium tuberculosis aerosol creates partial infection in mice. Tuberculosis
794 (Edinb). 2012;92(2):160-5. Epub 20111221. doi: 10.1016/j.tube.2011.11.007. PubMed
795 PMID: 22197183; PubMed Central PMCID: PMC3288716.
796 39. Rao C, Benhabib H, Ensminger AW. Phylogenetic reconstruction of the Legionella
797 pneumophila Philadelphia-1 laboratory strains through comparative genomics. PLoS One.
798 2013;8(5):e64129. Epub 20130522. doi: 10.1371/journal.pone.0064129. PubMed PMID:
799 23717549; PubMed Central PMCID: PMC3661481.
800 40. Molofsky AB, Byrne BG, Whitfield NN, Madigan CA, Fuse ET, Tateda K, et al.
801 Cytosolic recognition of flagellin by mouse macrophages restricts Legionella pneumophila
802 infection. J Exp Med. 2006;203(4):1093-104. Epub 20060410. doi: 10.1084/jem.20051659.
803 PubMed PMID: 16606669; PubMed Central PMCID: PMC1584282.
804 41. Ren T, Zamboni DS, Roy CR, Dietrich WF, Vance RE. Flagellin-deficient Legionella
805 mutants evade caspase-1- and Naip5-mediated macrophage immunity. PLoS Pathog.
806 2006;2(3):e18. Epub 20060317. doi: 10.1371/journal.ppat.0020018. PubMed PMID:
807 16552444; PubMed Central PMCID: PMC1401497.

42. Stoeckius M, Hafemeister C, Stephenson W, Houck-Loomis B, Chattopadhyay PK, Swerdlow H, et al. Simultaneous epitope and transcriptome measurement in single cells. Nat Methods. 2017;14(9):865-8. Epub 20170731. doi: 10.1038/nmeth.4380. PubMed PMID: 28759029; PubMed Central PMCID: PMC5669064.
43. Miller SA, Policastro RA, Sriramkumar S, Lai T, Huntington TD, Ladaika CA, et al. LSD1 and Aberrant DNA Methylation Mediate Persistence of Enteroendocrine Progenitors That Support. Cancer Res. 2021;81(14):3791-805. Epub 20210525. doi: 10.1158/0008-5472.CAN-20-3562. PubMed PMID: 34035083; PubMed Central PMCID: PMC8513805.
44. Liu D, Mai D, Jahn AN, Murray TA, Aitchison JD, Gern BH, et al. APOE protects against severe infection with Mycobacterium tuberculosis by restraining production of neutrophil extracellular traps. PLoS Pathog. 2025;21(6):e1013267. Epub 20250616. doi: 10.1371/journal.ppat.1013267. PubMed PMID: 40523023; PubMed Central PMCID: PMC12201663.
45. Lin PL, Ford CB, Coleman MT, Myers AJ, Gawande R, Ioerger T, et al. Sterilization of granulomas is common in active and latent tuberculosis despite within-host variability in bacterial killing. Nat Med. 2014;20(1):75-9. Epub 20131215. doi: 10.1038/nm.3412. PubMed PMID: 24336248; PubMed Central PMCID: PMC3947310.
46. MacMicking JD, Taylor GA, McKinney JD. Immune control of tuberculosis by IFN-gamma-inducible LRG-47. Science. 2003;302(5645):654-9. doi: 10.1126/science.1088063. PubMed PMID: 14576437.
47. Van Dis E, Fox DM, Morrison HM, Fines DM, Babirye JP, McCann LH, et al. IFN-γ-independent control of M. tuberculosis requires CD4 T cell-derived GM-CSF and activation of HIF-1α. PLoS Pathog. 2022;18(7):e1010721. Epub 20220725. doi: 10.1371/journal.ppat.1010721. PubMed PMID: 35877763; PubMed Central PMCID: PMC9352196.
48. Leal IS, Smedegård B, Andersen P, Appelberg R. Failure to induce enhanced protection against tuberculosis by increasing T-cell-dependent interferon-gamma generation. Immunology. 2001;104(2):157-61. doi: 10.1046/j.1365-2567.2001.01305.x. PubMed PMID: 11683955; PubMed Central PMCID: PMC1783293.
49. Sakai S, Kauffman KD, Sallin MA, Sharpe AH, Young HA, Ganusov VV, et al. CD4 T Cell-Derived IFN-γ Plays a Minimal Role in Control of Pulmonary Mycobacterium tuberculosis Infection and Must Be Actively Repressed by PD-1 to Prevent Lethal Disease. PLoS Pathog. 2016;12(5):e1005667. Epub 20160531. doi: 10.1371/journal.ppat.1005667. PubMed PMID: 27244558; PubMed Central PMCID: PMC4887085.
50. Srivastava S, Ernst JD. Cutting edge: Direct recognition of infected cells by CD4 T cells is required for control of intracellular Mycobacterium tuberculosis in vivo. J Immunol. 2013;191(3):1016-20. Epub 20130701. doi: 10.4049/jimmunol.1301236. PubMed PMID: 23817429; PubMed Central PMCID: PMC3725655.
51. Abel L, El-Baghdadi J, Bousfiha AA, Casanova JL, Schurr E. Human genetics of tuberculosis: a long and winding road. Philos Trans R Soc Lond B Biol Sci. 2014;369(1645):20130428. Epub 20140512. doi: 10.1098/rstb.2013.0428. PubMed PMID: 24821915; PubMed Central PMCID: PMC4024222.
52. Boisson-Dupuis S, Bustamante J. Mycobacterial diseases in patients with inborn errors of immunity. Curr Opin Immunol. 2021;72:262-71. Epub 20210724. doi:

10.1016/j.coi.2021.07.001. PubMed PMID: 34315005; PubMed Central PMCID: PMC9172628.
53. Azad AK, Sadee W, Schlesinger LS. Innate immune gene polymorphisms in tuberculosis. Infect Immun. 2012;80(10):3343-59. Epub 20120723. doi: 10.1128/IAI.00443-12. PubMed PMID: 22825450; PubMed Central PMCID: PMC3457569.
54. Setiabudiawan TP, Apriani L, Verrall AJ, Utami F, Schneider M, Indrati AR, et al. Immune correlates of early clearance of Mycobacterium tuberculosis among tuberculosis household contacts in Indonesia. Nat Commun. 2025;16(1):309. Epub 20250102. doi: 10.1038/s41467-024-55501-6. PubMed PMID: 39747050; PubMed Central PMCID: PMC11695729.
55. Lu LL, Smith MT, Yu KKQ, Luedemann C, Suscovich TJ, Grace PS, et al. IFN-γ-independent immune markers of Mycobacterium tuberculosis exposure. Nat Med. 2019;25(6):977-87. Epub 20190520. doi: 10.1038/s41591-019-0441-3. PubMed PMID: 31110348; PubMed Central PMCID: PMC6559862.
56. Dallmann-Sauer M, Fava VM, Malherbe ST, MacDonald CE, Orlova M, Kroon EE, et al. Mycobacterium tuberculosis resisters despite HIV exhibit activated T cells and macrophages in their pulmonary alveoli. J Clin Invest. 2025;135(7). Epub 20250121. doi: 10.1172/JCI188016. PubMed PMID: 39836471; PubMed Central PMCID: PMC11957701.
57. Li H, Wang XX, Wang B, Fu L, Liu G, Lu Y, et al. Latently and uninfected healthcare workers exposed to TB make protective antibodies against Mycobacterium tuberculosis. Proc Natl Acad Sci U S A. 2017;114(19):5023-8. Epub 20170424. doi: 10.1073/pnas.1611776114. PubMed PMID: 28438994; PubMed Central PMCID: PMC5441709.
58. Azuma M, Ito D, Yagita H, Okumura K, Phillips JH, Lanier LL, et al. B70 antigen is a second ligand for CTLA-4 and CD28. Nature. 1993;366(6450):76-9. doi: 10.1038/366076a0. PubMed PMID: 7694153.
59. Freeman GJ, Gribben JG, Boussiotis VA, Ng JW, Restivo VA, Lombard LA, et al. Cloning of B7-2: a CTLA-4 counter-receptor that costimulates human T cell proliferation. Science. 1993;262(5135):909-11. doi: 10.1126/science.7694363. PubMed PMID: 7694363.
60. Flores-Batista VC, Boechat N, Lago PM, Lazzarini LC, Pessanha LR, Almeida AS, et al. Low expression of antigen-presenting and costimulatory molecules by lung cells from tuberculosis patients. Braz J Med Biol Res. 2007;40(12):1671-9. Epub 20071029. doi: 10.1590/s0100-879x2006005000141. PubMed PMID: 17713660.
61. Vance RE. Tuberculosis as an unconventional interferonopathy. Curr Opin Immunol. 2025;92:102508. Epub 20241204. doi: 10.1016/j.coi.2024.102508. PubMed PMID: 39637776.
62. Zhang G, deWeerd NA, Stifter SA, Liu L, Zhou B, Wang W, et al. A proline deletion in IFNAR1 impairs IFN-signaling and underlies increased resistance to tuberculosis in humans. Nat Commun. 2018;9(1):85. Epub 20180108. doi: 10.1038/s41467-017-02611-z. PubMed PMID: 29311663; PubMed Central PMCID: PMCPMC5758831.
63. Moreira-Teixeira L, Mayer-Barber K, Sher A, O'Garra A. Type I interferons in tuberculosis: Foe and occasionally friend. J Exp Med. 2018;215(5):1273-85. Epub 20180417. doi: 10.1084/jem.20180325. PubMed PMID: 29666166; PubMed Central PMCID: PMCPMC5940272.

896 64. Witt KC, Dziulko A, An J, Pekovic F, Cheng AX, Liu GY, et al. SP140-RESIST pathway
897 regulates interferon mRNA stability and antiviral immunity. Nature. 2025;643(8074):1372-
898 80. Epub 20250611. doi: 10.1038/s41586-025-09152-2. PubMed PMID: 40500448; PubMed
899 Central PMCID: PMCPMC12310523.
900 65. Guarda G, Braun M, Staehli F, Tardivel A, Mattmann C, Förster I, et al. Type I
901 interferon inhibits interleukin-1 production and inflammasome activation. Immunity.
902 2011;34(2):213-23. doi: 10.1016/j.immuni.2011.02.006. PubMed PMID: 21349431.
903 66. Rayamajhi M, Humann J, Penheiter K, Andreasen K, Lenz LL. Induction of IFN-
904 alphabeta enables Listeria monocytogenes to suppress macrophage activation by IFN-
905 gamma. J Exp Med. 2010;207(2):327-37. Epub 20100201. doi: 10.1084/jem.20091746.
906 PubMed PMID: 20123961; PubMed Central PMCID: PMC2822610.
907 67. Stanley SA, Johndrow JE, Manzanillo P, Cox JS. The Type I IFN response to infection
908 with Mycobacterium tuberculosis requires ESX-1-mediated secretion and contributes to
909 pathogenesis. J Immunol. 2007;178(5):3143-52. doi: 10.4049/jimmunol.178.5.3143.
910 PubMed PMID: 17312162.
911 68. Lippmann J, Müller HC, Naujoks J, Tabeling C, Shin S, Witzenrath M, et al. Dissection
912 of a type I interferon pathway in controlling bacterial intracellular infection in mice. Cell
913 Microbiol. 2011;13(11):1668-82. Epub 20110824. doi: 10.1111/j.1462-5822.2011.01646.x.
914 PubMed PMID: 21790939; PubMed Central PMCID: PMC3196383.
915 69. Stetson DB, Medzhitov R. Recognition of cytosolic DNA activates an IRF3-
916 dependent innate immune response. Immunity. 2006;24(1):93-103. doi:
917 10.1016/j.immuni.2005.12.003. PubMed PMID: 16413926.
918 70. Voskuil MI, Bartek IL, Visconti K, Schoolnik GK. The response of mycobacterium
919 tuberculosis to reactive oxygen and nitrogen species. Front Microbiol. 2011;2:105. Epub
920 20110513. doi: 10.3389/fmicb.2011.00105. PubMed PMID: 21734908; PubMed Central
921 PMCID: PMC3119406.
922 71. Espich S, Berry S, Balakhmet A, Chang X, Thuong NTT, Dorajoo R, et al. Impaired
923 aldehyde detoxification caused by a common human polymorphism promotes anti-
924 bacterial immunity. bioRxiv. 2025. Epub Oct 18, 2025. doi:
925 *https://doi.org/10.1101/2023.08.24.554661*.
926 72. Thomas SM, Olive AJ. High Lethality of Mycobacterium tuberculosis Infection in
927 Mice Lacking the Phagocyte Oxidase and Caspase1/11. Infect Immun.
928 2023;91(7):e0006023. Epub 20230614. doi: 10.1128/iai.00060-23. PubMed PMID:
929 37314361; PubMed Central PMCID: PMCPMC10353354.
930 73. Darwin KH. Mycobacterium tuberculosis: the honey badger of pathogens. EMBO
931 Rep. 2021;22(9):e53619. Epub 20210728. doi: 10.15252/embr.202153619. PubMed PMID:
932 34322986; PubMed Central PMCID: PMC8419694.
933 74. Gordon C. The crazy nastyass honeybadger. Youtube.com2011. p.
934 https://www.youtube.com/watch?v=4r7wHMg5Yjg.
935 75. Kotov DI, Lee OV, Fattinger SA, Langner CA, Guillen JV, Peters JM, et al. Early cellular
936 mechanisms of type I interferon-driven susceptibility to tuberculosis. Cell.
937 2023;186(25):5536-53.e22. Epub 20231128. doi: 10.1016/j.cell.2023.11.002. PubMed
938 PMID: 38029747; PubMed Central PMCID: PMC10757650.
939 76. Mampel J, Spirig T, Weber SS, Haagensen JA, Molin S, Hilbi H. Planktonic replication
940 is essential for biofilm formation by Legionella pneumophila in a complex medium under

941 static and dynamic flow conditions. Appl Environ Microbiol. 2006;72(4):2885-95. doi:
942 10.1128/AEM.72.4.2885-2895.2006. PubMed PMID: 16597995; PubMed Central PMCID:
943 PMC1448985.

944